JAMES | Journal of Advances in Modeling Earth Systems®

RESEARCH ARTICLE
10.1029/2021MS002852

NASA GEOS Composition Forecast Modeling System GEOS-CF v1.0: Stratospheric Composition

K. E. Knowland[1,2,3], C. A. Keller[1,2,3], P. A. Wales[1,2,3], K. Wargan[2,4], L. Coy[2,4], M. S. Johnson[5], J. Liu[1,3,6], R. A. Lucchesi[2,4], S. D. Eastham[7,8], E. Fleming[4,6], Q. Liang[6], T. Leblanc[9], N. J. Livesey[10], K. A. Walker[11], L. E. Ott[2], and S. Pawson[2]

[1]Universities Space Research Association (USRA)/GESTAR, Columbia, MD, USA, [2]NASA Goddard Space Flight Center (GSFC), Global Modeling and Assimilation Office (GMAO), Greenbelt, MD, USA, [3]Now Morgan State University (MSU)/GESTAR-II, Baltimore, MD, USA, [4]Science Systems and Applications (SSAI), Inc., Lanham, MD, USA, [5]Earth Science Division, NASA Ames Research Center, Moffett Field, CA, USA, [6]Atmospheric Chemistry and Dynamics Laboratory, NASA GSFC, Greenbelt, MD, USA, [7]Laboratory for Aviation and the Environment, Department of Aeronautics and Astronautics, Massachusetts Institute of Technology, Cambridge, MA, USA, [8]Joint Program on the Science and Policy of Global Change, Massachusetts Institute of Technology, Cambridge, MA, USA, [9]Jet Propulsion Laboratory, California Institute of Technology, Wrightwood, CA, USA, [10]Jet Propulsion Laboratory, California Institute of Technology, Pasadena, CA, USA, [11]Department of Physics, University of Toronto, Toronto, ON, Canada

Abstract

The NASA Goddard Earth Observing System (GEOS) Composition Forecast (GEOS-CF) provides recent estimates and 5-day forecasts of atmospheric composition to the public in near-real time. To do this, the GEOS Earth system model is coupled with the GEOS-Chem tropospheric-stratospheric unified chemistry extension (UCX) to represent composition from the surface to the top of the GEOS atmosphere (0.01 hPa). The GEOS-CF system is described, including updates made to the GEOS-Chem UCX mechanism within GEOS-CF for improved representation of stratospheric chemistry. Comparisons are made against balloon, lidar, and satellite observations for stratospheric composition, including measurements of ozone (O_3) and important nitrogen and chlorine species related to stratospheric O_3 recovery. The GEOS-CF nudges the stratospheric O_3 toward the GEOS Forward Processing (GEOS FP) assimilated O_3 product; as a result the stratospheric O_3 in the GEOS-CF historical estimate agrees well with observations. During abnormal dynamical and chemical environments such as the 2020 polar vortexes, the GEOS-CF O_3 forecasts are more realistic than GEOS FP O_3 forecasts because of the inclusion of the complex GEOS-Chem UCX stratospheric chemistry. Overall, the spatial patterns of the GEOS-CF simulated concentrations of stratospheric composition agree well with satellite observations. However, there are notable biases—such as low NO_x and HNO_3 in the polar regions and generally low HCl throughout the stratosphere—and future improvements to the chemistry mechanism and emissions are discussed. GEOS-CF is a new tool for the research community and instrument teams observing trace gases in the stratosphere and troposphere, providing near-real-time three-dimensional gridded information on atmospheric composition.

Plain Language Summary

In the stratosphere, the ozone layer protects life on Earth from harmful ultraviolet, "UV," radiation. Chemical loss of this protective ozone occurs each year over Antarctica and occasionally over the Arctic during spring when air over these regions are cut-off from the rest of the stratosphere because of the strong winds blowing circularly around the pole. For accurate forecasting of the ozone layer and UV, it is critical to have both meteorology and chemistry accurately represented in forecast models. NASA's Goddard Earth Observing System composition forecast, "GEOS-CF," produces global 5-day forecasts of weather and atmospheric trace gases that are important for tracking the chemical interactions in the full atmosphere. Additionally, weather systems can bring down stratospheric ozone toward the Earth's surface where ozone is a regulated air pollutant. GEOS-CF can differentiate between ozone enhancements at the Earth's surface that result from pollution and from stratosphere-to-troposphere transport, improving the forecasts of stratospheric-influenced ozone exceedance events. This study describes the GEOS-CF model system and evaluates the modeled representation of stratospheric trace gases. GEOS-CF products are used to support NASA ground and satellite-based instrument teams as well as field and aircraft campaigns that measure trace gases throughout the atmosphere.

Key Points:

- Demonstrate the GEOS-CF system is capable of supporting NASA science missions and applications which observe stratospheric composition
- The GEOS-CF model produces realistic stratospheric ozone forecasts, a new capability during anomalous polar vortex conditions
- Spatial patterns of the GEOS-CF simulated concentrations of stratospheric composition agree well with independent observations

Supporting Information:

Supporting Information may be found in the online version of this article.

Correspondence to:

K. E. Knowland,
k.e.knowland@nasa.gov

Citation:

Knowland, K. E., Keller, C. A., Wales, P. A., Wargan, K., Coy, L., Johnson, M. S., et al. (2022). NASA GEOS Composition Forecast Modeling System GEOS-CF v1.0: Stratospheric composition. *Journal of Advances in Modeling Earth Systems*, *14*, e2021MS002852. https://doi.org/10.1029/2021MS002852

Received 30 SEP 2021
Accepted 13 APR 2022

1. Introduction

NASA's Global Modeling and Assimilation Office (GMAO) provides a suite of Goddard Earth Observing System (GEOS) model products to the public in near-real time (analyses and forecasts) and with a month to two-month latency (reanalysis; https://gmao.gsfc.nasa.gov/GMAO_products/). These products support NASA field missions and assess the impacts of NASA observations on environmental prediction. In order to support near-real-time NASA applications focused on atmospheric composition, it is essential GEOS has a realistic representation of stratospheric composition and chemistry (Nielsen et al., 2017). Ozone (O_3) is an important trace gas in the stratosphere where the total O_3 column acts to shield the Earth's surface from harmful ultra-violet (UV) radiation, while at the surface it is harmful to human health and vegetation (Krzyzanowski & Cohen, 2008; Schlink et al., 2006). Since the total column O_3 (TCO) varies from day-to-day depending on stratospheric conditions, forecasting TCO is an important input for accurate surface UV forecasts (Turner et al., 2017). The discovery of the Antarctic "Ozone hole" nearly 40 years ago by ground-based, sonde and satellite measurements (e.g., Farman et al., 1985; Solomon et al., 1986; Stolarski et al., 1986) indicated decreases in the ozone layer were greater than the 1% per decade that early models were predicting (Bhartia & McPeters, 2018). Tracking the recovery of the Antarctic ozone hole requires the sustained combination of high quality observations and models.

The GMAO has a mature data assimilation system (DAS) within GEOS to provide a realistic global three-dimentional (3D) stratospheric O_3 product for the "satellite era" (since 1980) (Wargan et al., 2015, 2017; Wargan, Kramarova, et al., 2020; Wargan, Weir, et al., 2020) which can be used in analysis of stratospheric O_3 trends (Wargan et al., 2018). For 5–10 day TCO forecasting, GMAO's state-of-the-science numerical weather prediction GEOS Forward Processing (GEOS FP; Lucchesi, 2018) system first assimilates near-real time O_3 observations (Figure S1a in Supporting Information S1). However, the GEOS FP forecasts rely on simple parameterized chemistry based on fixed, pre-calculated, monthly, latitude/altitude production and loss values as described in Nielsen et al. (2017). The GEOS FP forecasts fail when TCO is far from climatological values.

To further support the research community and NASA missions with atmospheric composition simulations, GMAO expanded the GEOS capabilities with the state-of-the-science GEOS-Chem chemistry transport model (CTM; Bey et al., 2001) fully integrated into GEOS (Hu et al., 2018; Keller et al., 2014; Long et al., 2015). Owing to the complexity of the chemistry, this coupled configuration (Figure S1b in Supporting Information S1) is run once daily and provides near-real time estimates of recent atmospheric composition and detailed composition forecasts ("GEOS-CF") of the 3D state of the atmosphere on the same spatial (0.25°) resolution as the meteorology (Keller et al., 2021). For GEOS-CF, the combination of the sophisticated GEOS-Chem chemistry within a GEOS forecasting system allows for improved forecasting of TCO when far from climatological values and, for the first time, provides near-real time 3D estimates of chemical species that are critical for understanding stratospheric O_3 recovery and loss, such as nitrogen oxides (NO_x) and hydrogen chloride (HCl). This current study evaluating the GEOS-CF stratospheric composition (100–1 hPa) is a companion paper to the GEOS-CF description paper by Keller et al. (2021) which evaluated tropospheric composition and surface air quality forecast skill against independent observations.

The GEOS-Chem CTM is a global 3D CTM driven by assimilated GEOS meteorological fields (Bey et al., 2001). It has an extensive community of developers and users worldwide (http://acmg.seas.harvard.edu/geos/). As the tropospheric chemistry became increasingly more sophisticated in GEOS-Chem, the stratospheric chemical boundary condition became a limiting factor for stratosphere-troposphere coupling analysis (Eastham et al., 2014). Over a similar time frame, the NASA Global Modeling Initiative (GMI) chemistry mechanism was developed at NASA Goddard Space Flight Center and is maintained to be state-of-the-science for stratospheric chemistry modeling to support policy relevant assessments on stratospheric composition and O_3 recovery (e.g., Bucsela et al., 2013; Douglass et al., 1999, 2004; Duncan et al., 2007; Kinnison et al., 2001; Nielsen et al., 2017; Rotman et al., 2001; Strahan & Douglass, 2018). Using a version of the NASA GMI stratospheric chemistry mechanism, updated with the Jet Propulsion Laboratory (JPL)'s stratospheric recommendations for kinetic and photochemical data (JPL Publication 10-06; Sander et al., 2011), Eastham et al. (2014) extended GEOS-Chem to have the capability to run with a unified tropospheric and stratospheric chemistry mechanism, "UCX." The GEOS-Chem CTM has continued to evolve since the version 9 evaluated in Eastham et al. (2014), with updates which could impact stratospheric composition such as the treatment of halogen species (Chen et al., 2017; Schmidt et al., 2016; Sherwen, Evans, et al., 2016; Sherwen, Schmidt, et al., 2016). This present study benchmarks the stratospheric composition using a more recent version of GEOS-Chem (version 12.0.1) run in an online high-resolution global

GEOS simulation (GEOS-CF) to assess the readiness of GEOS-CF output to support the research community and to prioritize needed improvements.

The paper follows with an overview of the GEOS-CF version 1.0 ("v1") system as described by Keller et al. (2021) in Section 2, followed by the description of the independent observations—those which do not constrain the GEOS-CF constituent concentrations—in Section 3 that are used for validation of stratospheric composition in Sections 4–6. After initial evaluation of the GEOS-CF v1 stratospheric composition, several updates were made to the UCX code mid-production, which are outlined in Section 4. The evaluation of the updated system against ozonesondes, lidar and satellite observations for the year 2020 is presented in Section 5, with case studies of forecast skill in Section 6. Final summary and future developments are discussed in Section 7.

2. GEOS Composition Forecast (GEOS-CF) System Description

The NASA GEOS-CF system (Keller et al., 2021) is a near-real time global 3D coupled chemistry and meteorology modeling system with the offline GEOS-Chem CTM code fully integrated as a chemistry module in GEOS (Hu et al., 2018; Long et al., 2015). The GEOS-Chem chemistry components are therefore the same in GEOS-CF as in the offline CTM except the dynamics and turbulence schemes use the online GEOS meteorology instead of the offline transport scheme within the CTM. Briefly, the GEOS-CF configuration has the GEOS atmospheric general circulation model (AGCM; Molod et al., 2015) one-way coupled to the GEOS-Chem chemistry module (Figure S1b in Supporting Information S1), run on a cube-sphere horizontal grid at c360 resolution and on 72 GEOS hybrid-eta model layers from the surface to 0.01 hPa, with output at the global resolution of 0.25° latitude × 0.25° longitude (GEOS-CF v1; Keller et al., 2021).

The addition of stratospheric chemistry in GEOS-Chem through UCX (Eastham et al., 2014) includes: stratospheric chemical reactions present in GMI, methane changed from a fixed background value to an advected tracer, and shorter wavelengths in the Fast-JX photolysis solver. Also, surface boundary conditions for nitrous oxide (N_2O) and several ozone-depleting substances (ODS; e.g., halogen bromine (Br) and chlorine (Cl) species) were defined following the World Meteorological Organization (WMO) 2006 ozone assessment (Daniel et al., 2006), and a surface boundary condition of 500 ppt was set for carbonyl sulphide (OCS), a precursor for sulfate aerosols (Weisenstein et al., 1997). Lastly, UCX includes treatments of stratospheric sulfate aerosols (Carslaw et al., 1997) and polar stratospheric clouds (PSCs; Kirner et al., 2011) on which heterogeneous reactions can occur and lead to seasonal O_3 depletion in the stratosphere. Additional details regarding the representation of stratospheric chemistry and physics are provided in Eastham et al. (2014). Modifications to UCX and boundary conditions used in this work are described in Section 4.

Since the GEOS-CF configuration is computationally expensive due to the complexity of the chemistry, instead of running a full DAS, GEOS-CF relies on GMAO's meteorological "replay" technique (Orbe et al., 2017), where the AGCM computes the increments for pressure, temperature, wind (U, V), specific humidity, aerosol optical depth and O_3 based on pre-computed analysis fields from a previously run assimilation system (Figures S1a and S1b in Supporting Information S1). Every day, prior to the launch of the forecast, GEOS-CF replays to the past 24-hr of GEOS FP for Instrument Teams (GEOS FP-IT; Lucchesi, 2015) assimilated meteorology, aerosols and O_3 in order to ensure consistent model physics within the AGCM (Figures S1a and S1b in Supporting Information S1; see Figure 1, Keller et al., 2021). Unlike GEOS FP, GEOS FP-IT is a static model system, designed to have minimal updates to the system in order to support near-real time retrievals by satellite instrument teams. For similar reasons, a "frozen" model was preferred as the driving meteorology for GEOS-CF v1. It is important to note that in GEOS-CF the GEOS-Chem aerosols and O_3 are run passively, that is with no radiation interaction with the meteorology, and therefore do not directly impact the dynamics nor are the increments applied to the GEOS-Chem aerosols and O_3.

In the GEOS-CF v1, there is no direct data assimilation of chemical species; however, near-real time satellite observations of (a) fire radiative power and (b) stratospheric O_3 are incorporated into GEOS-CF during the replay segments. Specifically: (a) the Quick Fire Emissions Data set (QFED; Darmenov & da Silva, 2015) informs the model of recent fires, which is then persisted forward for each 5-day forecast and (b) the GEOS-CF stratospheric O_3 (pressures less than approximately 56 hPa) is nudged toward the GEOS FP assimilated O_3 3-hourly average product (Figure S1b in Supporting Information S1). The GEOS FP O_3 observing system includes the limb-sounding profiles from the near-real time Microwave Limb Sounder (MLS; Waters et al., 2006) product,

Table 1
Overview of Observation Data Sets Used for GEOS-CF Model Validation

Description	Species	Reference
Satellite		
ACE-FTS v4.1	O_3, H_2O, HCl, HNO_3, N_2O, NO, NO_2, N_2O_5, $ClONO_2$	Boone et al. (2020)
MLS v5	O_3, H_2O, HCl, HNO_3, N_2O	Livesey et al. (2020)
SAGE III/ISS v5.1	O_3	McCormick et al. (2020) and H. J. R. Wang et al. (2020)
Ozone Watch	O_3	https://ozonewatch.gsfc.nasa.gov/
OMI "TOMS-like" v3 level 3 product	O_3	McPeters et al. (2008) and Bhartia (2012)
SBUV Merged Ozone product v8.6	O_3	Frith et al. (2014)
Balloon		
Ozonesondes	O_3	http://www.woudc.org, ftp://aftp.cmdl.noaa.gov/data/ozwv/ozonesonde/
Ground-based		
TOLNet Lidar	O_3	https://www-air.larc.nasa.gov/missions/TOLNet

column-based measurements from Ozone Monitoring Instrument (OMI; Levelt et al., 2006, 2018) and, after March 2019, the O_3 observing system was updated to include TCO from Ozone Mapping and Profiler Suite Nadir Mapper (OMPS-NM; Bak et al., 2017) instrument aboard Suomi National Polar-Orbiting Partnership. The nudging method is intended to keep stratospheric O_3 in line with observations on a seasonal time scale while still allowing GEOS-Chem to simulate complex chemical interactions in the troposphere and stratosphere. The nudging technique in GEOS-CF v1 is as follows: from the top of the atmosphere (GEOS level 1) down to lower stratosphere (GEOS level 33, approximately 40 hPa), the O_3 is nudged 20% toward the GEOS FP O_3 every 3 hr. There is not a hard cut off in the nudging, but instead from levels 33 to 35 (approximately 56 hPa, well above the tropopause), there is a smooth transition, and then from GEOS level 35 to 72 (model's lowest layer), the O_3 is not constrained.

This replay set-up provides the best initial conditions for the 5-day forecast initialized at 12:00 UTC (See Figure 1 of Keller et al. [2021]). Since the end of each replay segment is used to start the next day's replay simulation, these 24-hr segments can be considered as a continuous model best estimate of the 3D composition of the atmosphere, starting 1 January 2018 for GEOS-CF v1. The GEOS-CF 5-day forecasts remain available to the public for a 2-week period, and are archived at the NASA Center for Climate Simulation (NCCS) for posterity. Full details of the GEOS-CF model set-up, including emission data sets, and available model output can be found in Keller et al. (2021) and Knowland et al. (2022), respectively.

3. Data

In this section, the remote-sensing and balloon-based observation data sets used (Table 1) for evaluation of the updates to GEOS-Chem UCX within GEOS-CF (Section 4) and the GEOS-CF stratospheric constituents for the year 2020 (Sections 5–6) following the applied updates are described. In this study, the GEOS-CF replay estimates of stratospheric composition for O_3, HCl, chlorine monoxide (ClO), nitric acid (HNO_3), N_2O, NO_y (sum of nitric oxide (NO), nitrogen dioxide (NO_2), HNO_3, chlorine nitrate ($ClONO_2$), and two dinitrogen pentoxide (N_2O_5)) and water vapor (H_2O) will be the main focus of the evaluation. While there are about 40 chemical species available on stratospheric levels from GEOS-CF, the analysis is limited to O_3 and key observable species related to O_3 chemistry. Within the GEOS-CF v1 forecast segment, the model output is reduced to only 2D diagnostics (e.g., TCO) and limited 3D output focusing on tropospheric and lower stratospheric composition. In Section 6, the forecast skill for TCO will be presented for two case study periods and an example of forecasting the impact of stratospheric O_3 on tropospheric composition is reported.

This manuscript focuses on the satellite observations and the global distribution of ozonesondes that can be used to make general conclusions about the global state of the stratospheric composition in GEOS-CF. Comparisons

against regional networks such as the Pandora network or the Tropospheric Ozone Lidar Network (TOLNet) are active areas of research (e.g., Dacic et al., 2020; Gronoff et al., 2021; Johnson et al., 2021; Robinson et al., 2020) as demonstrated with a case study using TOLNet vertically resolved O_3 measurements (Section 6.3).

3.1. Satellite

In addition to limb-sounding O_3 profiles, MLS observes other constituents which are useful for monitoring ODSs and atmospheric circulation to a sufficient quality on a profile-by-profile bases (Livesey et al., 2020). In this study, MLS level 2, version 5 (Livesey et al., 2020) profiles of O_3, H_2O, HCl, ClO, HNO_3, and N_2O for 2020 are used (Table 1). For MLS O_3, data within half an hour of the synoptic times (00:00, 6:00, 12:00, 18:00 UTC) are co-located with the GEOS-CF instantaneous O_3 for January–December 2020 (Figure 5). For zonal and global comparisons of MLS HCl, HNO_3, N_2O, and H_2O, only the MLS data within half an hour of 12:00 UTC are co-located to the 12:00 UTC instantaneous GEOS-CF 3D concentrations (Figures 7 and 11; Figures S4 and S6 in Supporting Information S1). The GEOS-CF outputs MLS observed species on 39 approximate MLS pressure levels from 316 to 0.0215 hPa (Knowland et al., 2022) to support comparisons to MLS profiles. For the polar vortex comparison (Figure 8), all available MLS data in that region were used and the profiles interpolated to three isentropic surfaces.

Other independent observations for model evaluation include measurements from two solar occultation instruments: the Stratospheric Aerosol and Gas Experiment (SAGE) III instrument aboard the International Space Station (ISS) and the Atmospheric Chemistry Experiment-Fourier Transform Spectrometer (ACE-FTS) on the Canadian SCISAT satellite. The solar occultation measurements from SAGE III/ISS (June 2017–present; Cisewski et al., 2014) and ACE-FTS (February 2004–present; Bernath, 2017; Bernath et al., 2005) provide high vertical resolution profiles of O_3, H_2O and other species but there are far fewer observations per day (15–30) compared to MLS profiles (3500). SAGE III/ISS has a measurement range from about 70°S to 70°N (H. J. R. Wang et al., 2020) while ACE-FTS covers further into the polar regions because of its high orbital inclination (74° compared to 52° for the ISS). The measurements are mainly in the stratosphere, however the retrieved profiles can be extended into the troposphere (generally limited to the cloud top height; Boone et al., 2020; Mauldin et al., 1998) and into the mesosphere (SAGE III/ISS; Mauldin et al., 1998; McCormick & Chu, 2004) and lower thermosphere (ACE-FTS; Boone et al., 2020). Here, SAGE III/ISS version 5.1 and ACE-FTS version 4.1 profiles are used. The O_3 profiles from both instruments were interpolated to the GEOS-CF "MLS pressure levels" and profiles ±30 min of each hour were selected for comparisons to the GEOS-CF hourly instantaneous O_3 on MLS pressure levels. For the additional chemical species which are not reported by MLS but are reported by ACE-FTS, the GEOS-CF 3D 3-hourly, instantaneous output on 35 isentropic surfaces (from 270 to 3000 K; Knowland et al., 2022) are compared to ACE-FTS measurements. The ACE-FTS observations were interpolated to isentropic surfaces from 330 to 1600 K for the comparison and the GEOS-CF isentropic output within 1.5 hr of the ACE-FTS measurements are selected.

Along with the satellite level 2 products for the instruments detailed above, publicly available O_3 values from the NASA "Ozone Watch" website (https://ozonewatch.gsfc.nasa.gov/) are used for verification of O_3 forecasts. Ozone Watch daily values of the Northern Hemisphere (NH) polar cap total O_3 and the Southern Hemisphere (SH) ozone hole area are historically based on a wide range of satellite observations; since July 2016 it is based on the OMPS-NM. If OMPS-NM data is missing, the Ozone Watch product relies on the near-real time GEOS FP assimilated TCO product. Merged, homogenized satellite products are useful for evaluation of long-term simulations since biases across multiple instruments are removed relative to a reference data set. We use two merged products—version 8.6 of the SBUV Merged Ozone Data set (Frith et al., 2014) and version 3 of the OMI "TOMS-like" level 3 gridded product (Bhartia, 2012; McPeters et al., 2008)—for evaluation of the GEOS Chemistry Climate Model (GEOS CCM; Nielsen et al., 2017) simulated TCO and GEOS-CF TCO (see Section 4).

3.2. Ozonesonde Observations

Ozonesondes provide profile measurements of tropospheric and stratospheric O_3, up to about 30–35 km altitude (Stauffer et al., 2020; Sterling et al., 2018; Thompson et al., 2017). Data was selected from 20 of the 24 sites in Keller et al. (2021), distributed globally (Table 2, Figure S2 in Supporting Information S1), and accessed through the World Ozone and Ultraviolet Data Center (WOUDC, http://www.woudc.org) and from Global

Table 2
Ozonesonde Launch Locations, Listed From North to South, Grouped Into Five Latitude Bands (See Also Figure S2 in Supporting Information S1): NH Polar (>60°), NH Mid-Latitudes (30°–60°), Subtropics/Tropics (−30° to 30°), SH Mid-Latitudes (−30 to −60°) and SH Polar (<−60°)

Station name	Latitude (°N)	Longitude (°E)	Launch hour (UTC)	*N* (2020 only)
NH polar				
Alert	82.5	−62.3	18 or 23	17
Eureka	80.0	−85.9	11, 18 or 23	65
NH mid-latitudes				
Legionowo	52.4	21.0	11	41
Valentia	51.9	−10.2	11	30
Uccle	50.8	4.3	11–12	144
Praha	50.0	14.4	11	46
Payerne	46.5	6.6	10–12	111
Trinidad Head	41.1	−124.2	16–21	45
Madrid	40.5	−3.6	10–11	54
Boulder	40.0	−105.2	16–21	59
Tateno	36.1	140.1	14–15	37
Subtropics/tropics				
King's Park	22.3	114.2	5	48
Hilo	19.7	−155.1	18–19	50
Pago Pago	−14.3	−170.7	14–24	38
Suva	−18.1	178.4	21–23	15
SH mid-latitudes				
Broadmeadows	−37.7	144.9	0–3	51
Lauder	−45.0	169.7	19–8	54
Macquarie Island	−54.4	158.9	5 or 23	51
SH polar				
Syowa	−69.0	39.6	2, 8 or 14	46
South Pole	−90.0	169.0	8–11, 20–22	51

Note. Number of launches (*N*) for January–December 2020 are provided.

Monitoring Laboratory, National Oceanic and Atmospheric Administration (NOAA) network (ftp://aftp.cmdl.noaa.gov/data/ozwv/ozonesonde/). Keller et al. (2021) reported on the tropospheric portion of the profiles (1,000–200 hPa) for 2018–2019; this study focuses on stratospheric composition and will evaluate the profiles from 400 to 10 hPa. De Bilt, Pohang, Paramaribo, and Marambio were excluded from this study, as sites were selected using the criteria that each location has at least one observation reported in each month, similar to Steinbrecht et al. (2021). The number of ozonesonde launches in 2020 compared to the number of launches in previous years was reduced at many stations because of COVID-19 restrictions; nonetheless, there were still enough measurements for scientific study at the selected 20 stations (Table 2). At these sites, the frequency of ozonesonde launches is generally once or twice per week, and covers a range of launch times (Table 2).

The vertical resolution of the ozonesonde profiles (often >2,000 pressure levels) is reduced by interpolating the ozonesonde data onto 200 constant pressure levels from 1,000 to 10 hPa.

For comparisons, the model data are selected for the closest hour to the launch hour and then the closest grid-box to the ozonesonde station location. Furthermore, the model output is interpolated from the native resolution to the 200 constant pressure levels to match the sonde resolution, as was done in Keller et al. (2021).

3.3. TOLNet Ozone Lidars

In addition to comparisons against sounding data, the capability of the NASA GEOS-CF model to simulate and forecast the impact of stratospheric O_3 on tropospheric atmospheric composition can be assessed by comparing the GEOS-CF model output to observations from TOLNet. TOLNet is a network of 8 tropospheric O_3 lidars distributed throughout North America supported by NASA and NOAA (https://www-air.larc.nasa.gov/missions/TOLNet). These ground-based lidars provide Differential Absorption Lidar (DIAL)-derived, high vertical and temporal resolution, observations of tropospheric O_3 with high accuracy and precision continuously for many hours or even days (Leblanc et al., 2018; L. Wang et al., 2017). While Keller et al. (2021) found on average the NH free tropospheric O_3 was biased low compared to ozonesondes for 2018–2019, there is demonstrable synergy between the data from these lidar systems and the vertical structure of O_3 concentrations simulated by GEOS-CF (Dacic et al., 2020; Johnson et al., 2021), including episodic events when stratospheric O_3 descends to lower altitudes into the troposphere (Gronoff et al., 2021).

For this study, observations from the NASA JPL Table Mountain Facility (TMF) tropospheric O_3 lidar (TMTOL; McDermid et al., 2002), located in the San Gabriel Mountains near Los Angeles, California (34.38°N, 117.68°W) at an elevation of 2,285 m above sea level (asl) are used. This system has the capability to conduct continuous observations for multiple hours or days (Chouza et al., 2019) providing O_3 measurements from 100 m above ground level (agl) to the tropopause. For a qualitative comparison to GEOS-CF for the case study in Section 6.3, the lidar data is averaged hourly with 30 m vertical resolution.

4. Model Updates to GEOS-Chem UCX for GEOS-CF

Early evaluation of GEOS-CF v1 in 2018 against MLS observations indicated that GEOS-CF had significant biases in the stratosphere (not shown), caused by inaccurate initial conditions of ODSs as well as erroneous stratospheric removal of NO_x. Though the irregular stratospheric concentrations and distribution of some of the species had limited impact on the main observable tropospheric pollutants (Keller et al., 2021), it was critical that the

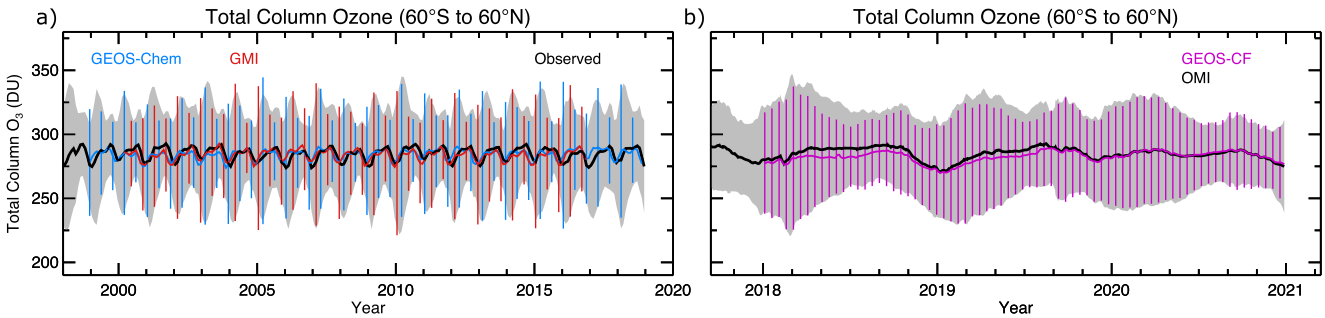

Figure 1. Near-global average (60°S–60°N) TCO (a) monthly mean for the GEOS-Chem GEOS CCM free-running simulation (1999–2018; blue), GMI GEOS CCM free-running simulation (2000–2016; red), and the SBUV Merged O_3 Data Set (1998–2018, black). Vertical lines and gray shaded region represent the standard deviation about the monthly mean for the GEOS CCM simulations and observations, respectively, and (b) daily mean from OMI "TOMS-like" level 3 gridded product (Bhartia, 2012; McPeters et al., 2008, 7-day running mean, black line; standard deviation, gray shading) and GEOS-CF (7-day running mean, magenta line; standard deviation, magenta vertical lines) for the region from 60°S to 60°N.

state of the GEOS-CF stratosphere be addressed in order to be a suitable product for supporting NASA campaigns and remote-sensing instruments which require realistic stratospheric composition. To do so, parallel long-term free-running (i.e., no meteorological replay) GEOS CCM simulations using the two troposphere-stratosphere chemistry mechanisms—GMI and GEOS-Chem—were performed (Figure S1c in Supporting Information S1) to assess the GEOS-Chem UCX stratospheric chemistry against the established GMI chemistry. This analysis confirmed that a well spun up GEOS-Chem stratosphere does lie within the observable TCO range (Figure 1a).

From the comparison of these two long-term free-running GEOS CCM simulations, four major updates were made to the GEOS-Chem UCX code base in GEOS-CF to be more in line with the GMI mechanism since Eastham et al. (2014). In addition, two more changes were made to improve the O_3 nudging technique and the run-time performance. Finally, the GEOS-CF stratospheric concentration fields were updated using the well-spun up (20-year) GEOS-Chem GEOS CCM simulation (blue line, Figure 1a). The updates and new initial conditions were implemented in the GEOS-CF near-real time system on 31 July 2019. The four major updates to the GEOS-Chem UCX code are:

First, the stratospheric photolysis and reaction rate constants were updated from JPL Publication 10–16 (Sander et al., 2011) to follow recommendations provided by a more recent release of the JPL kinetic evaluation (JPL Publication 15-10; Burkholder et al., 2015). The surface mixing ratio boundary conditions for ODSs were updated from the WMO 2006 ozone assessment to follow the newer baseline emission scenario from the WMO 2018 ozone assessment (Carpenter & Daniel, 2018). This update includes changing the methyl bromide (CH_3Br) boundary conditions to follow the WMO 2018 scenario rather than fixed zonal mean values (Parrella et al., 2012). Surface mixing ratio boundary conditions for N_2O in GEOS-CF are taken from the Representative Concentration Pathway 6.0 scenario for the fifth assessment report of the Intergovernmental Panel on Climate Change (Collins et al., 2013). The original evaluation of the UCX stratosphere was conducted using the GEOS-Chem version 9.01.03 mechanism that had a detailed tropospheric bromine mechanism (Parrella et al., 2012). In addition the updates to the ODS boundary conditions outlined above, the GEOS-Chem version (v12.0.1) used by GEOS-CF v1 includes updates to the tropospheric halogen mechanism that impact the quantity of Cl and Br species reaching the stratosphere (Chen et al., 2017; Schmidt et al., 2016; Sherwen, Schmidt, et al., 2016). In GEOS-CF v1, the mean annual stratospheric total Cl and Br content for 2020 are 3.0 ppb and 19 ppt, respectively, in general agreement with the stratospheric supply estimated by Engel and Rigby (2018). The amount of Cl supplied to the stratosphere by tropospheric total inorganic Cl (Cl_y) and VSLS is minor, less than 2%. Based on simulated mixing ratios at the tropical tropopause pressure, 5.6 ± 0.2 ppt of Br is supplied to the stratosphere by tropospheric Br_y and VSLS, in agreement with the previous modeling studies and aircraft observations summarized by the WMO 2018 Ozone Assessment (Engel & Rigby, 2018).

Second, more bromine was activated in GEOS-Chem than in the GMI simulations, contributing to greater O_3 loss in the lower stratosphere than observed, especially at low and mid-latitudes (see Figure 1b). Two heterogeneous reactions on PSCs (reactions 1 and 2) and three reactions on stratospheric sulfate aerosols (reactions 1–3) were identified as not included in GMI and subsequently turned off in GEOS-CF. These reactions are:

$$ClONO_2(g) + HBr(l, s) \rightarrow BrCl + HNO_3 \quad (1)$$

$$HOCl(g) + HBr(l, s) \rightarrow BrCl + H_2O \quad (2)$$

$$BrONO_2(g) + HCl(l, s) \rightarrow BrCl + HNO_3 \quad (3)$$

The heterogeneous reaction 1 between $ClONO_2$ and hydrogen bromide (HBr) on PSC surfaces was investigated by Hanson and Ravishankara (1992), but this reaction is disabled in the GEOS-CF system to be consistent with the GMI mechanism. Additionally, Burkholder et al. (2015) recommends that additional studies are needed to properly represent reaction 2, and laboratory analysis suggests that bromine nitrate ($BrONO_2$) and HCl do not directly react via reaction 3 (Hanson & Ravishankara, 1995).

Third, the family transport of Cl_y and Br_y species is implemented in GEOS-CF as described by Douglass et al. (2004) for GMI. When halogen species are transported individually, Douglass et al. (2004) identified errors in the advection scheme along sharp gradients between sunlit and nighttime mixing ratios. These advection errors resulted in nonphysical maxima in mixing ratios of Cl_y and Br_y that were detected in earlier versions of the GEOS-CF stratosphere. Since the total quantities of Cl_y and Br_y do not have sharp day to night gradients, implementing family transport removes occurrences of nonphysical maxima in halogen families in GEOS-CF v1.

Fourth, the solar zenith angle (SZA) in the photolysis calculations was updated to go beyond 90°, thereby accounting for twilight conditions important for chemistry simulations in the stratosphere and mesosphere. GEOS-Chem version 12.0.1 and GEOS-CF now truncate the SZA at 98° as done in GMI and allowed for in the Fast-Jx photolysis calculations. Previous versions of GEOS-Chem truncated the SZA at 90°, which resulted in longer nighttime conditions and sharpened the day-night constituent gradients across the terminator. This contributed to the non-physical advection errors in the Br_y and Cl_y species described above.

In addition to the new initial conditions for GEOS-CF stratospheric concentration fields using the well-spun up (20-year) GEOS-Chem GEOS CCM simulation, two more adjustments were made to the GEOS-CF v1 system: (a) the start of the transition layer for the O_3 nudging was raised from GEOS level 38 (approximately 90 hPa) to GEOS level 35 (approximately 56 hPa as described in Section 2) in order to make sure no GEOS FP O_3 was mistakenly added to the upper-troposphere since the nudging method does not differentiate between the stratosphere and troposphere; and (b) in the original version of GEOS-CF, GEOS-Chem UCX does explicit chemistry up to the stratopause and mesospheric chemistry is parameterized based on pre-defined production and loss rates. To speed up the run time of the GEOS-CF system, the mesospheric parameterization was disabled and stratospheric chemistry now extends up through the top of the GEOS atmosphere, thus avoiding the need to repeatedly read in production and loss rates. Note, this study is only evaluating stratospheric composition, considering concentrations up to 1 hPa.

For the evaluation of the GEOS-CF stratospheric composition in the following sections the focus is on only the 12-month period in 2020, after allowing several months for the stratosphere to stabilize. One can see an improved agreement in the (non-polar) TCO between GEOS-CF and OMI from late 2019 onwards in Figure 1b. Prior to the inclusion of the above outlined updates on 31 July 2019, GEOS-CF mean non-polar TCO is biased-low, and any analysis of the total column diagnostics or 3D stratospheric output from GEOS-CF v1 for this earlier period of the record should consider the potential biases from the stratospheric portion of the column.

It is unlikely that changes to atmospheric composition in 2020 from the COVID-19 pandemic restrictions impacted stratospheric composition significantly. For this reason, it is suitable to focus on the year 2020 for this study. Numerous studies investigated how the global COVID-19 pandemic restrictions impacted surface air quality through a reduction in anthropogenic emissions (an extensive collated list available at https://amigo.aeronomie.be/index.php/covid-19-publications/peer-reviewed); however, there are relatively few which explore the impact on free tropospheric (FT) composition—for example, Steinbrecht et al. (2021) and Clark et al. (2021) report moderate decreases of 7% NH FT O_3 for April–August 2020 and up to 12% in FT O_3 over Frankfurt during March–July 2020, respectively—and no studies to our knowledge with a focus on the stratosphere. While the reduction in air traffic from the grounding of a substantial portion of passenger aircraft (Clark et al., 2021; Le Quéré et al., 2020) likely led to a decrease in O_3-precursor emissions at cruising altitudes in the upper troposphere and lower stratosphere (UTLS), it is likely the anomalously low NH springtime O_3 in the stratospheric polar vortex is the greater driver in UTLS composition anomalies than the pandemic-related emission reductions (see

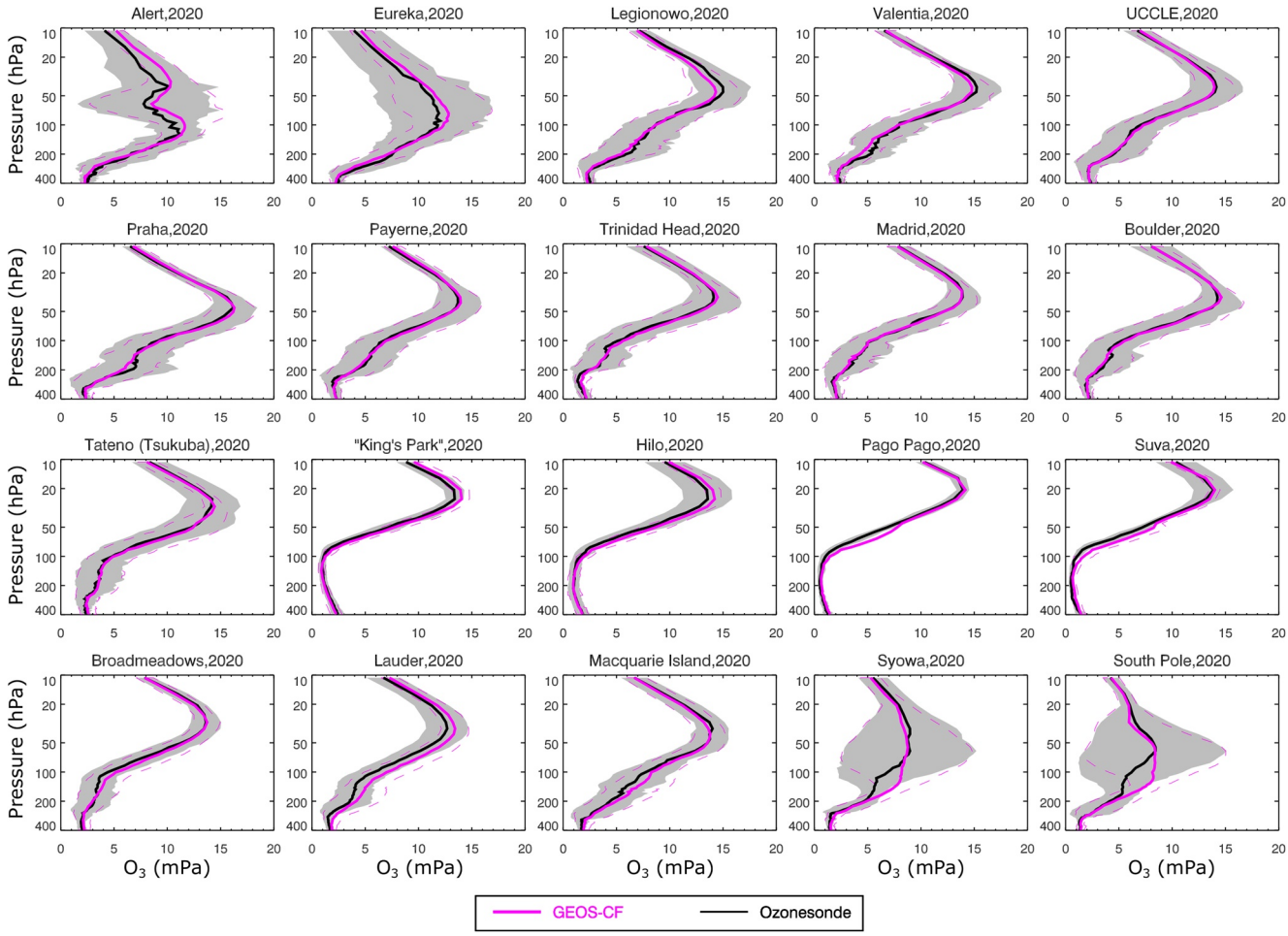

Figure 2. Median ozonesonde profiles (O_3, mPa) restricted to pressure levels between 400 and 10 hPa at 20 global stations for launches in January–December 2020 (median, black line; interquartile range, gray shading) compared to median GEOS-CF O_3 profiles (median, magenta solid line; interquartile range, magenta dashed lines). GEOS-CF profiles selected for the grid-box and time closest to the ozonesonde measurements. Launch locations displayed in order from North to South, as listed in Table 2.

Figure 3, Steinbrecht et al., 2021). The anomalous polar vortex circulation and chemistry in the NH (January–May 2020) and the SH (May–September 2020), both of interest to stratospheric chemists, will be discussed in detail throughout Sections 5–6.

5. Evaluation of GEOS-CF Stratospheric Composition in Replay Mode

In this section, the spatial distribution and variations for stratospheric O_3 (Section 5.1) and several species important for O_3 chemistry (Section 5.2) are evaluated against independent observations and related to the complexity of chemistry and emissions. Once the state of the GEOS-CF stratospheric composition with analyzed meteorology is established, applications of the GEOS-CF forecasts are presented (Section 6).

5.1. Ozone

Since the GEOS-CF stratospheric O_3 is constrained during the replay segment by the GEOS FP O_3 product which assimilates MLS, OMI and OMPS-NM O_3 observations, independent profile observations from ozonesondes, ACE-FTS, and SAGE III/ISS are used for validation with a comparison to MLS included.

In general, the median stratospheric O_3 simulated in GEOS-CF for the period between January through December 2020 agrees well with the median ozonesonde profiles (Figure 2) with median percent bias within ±20% through

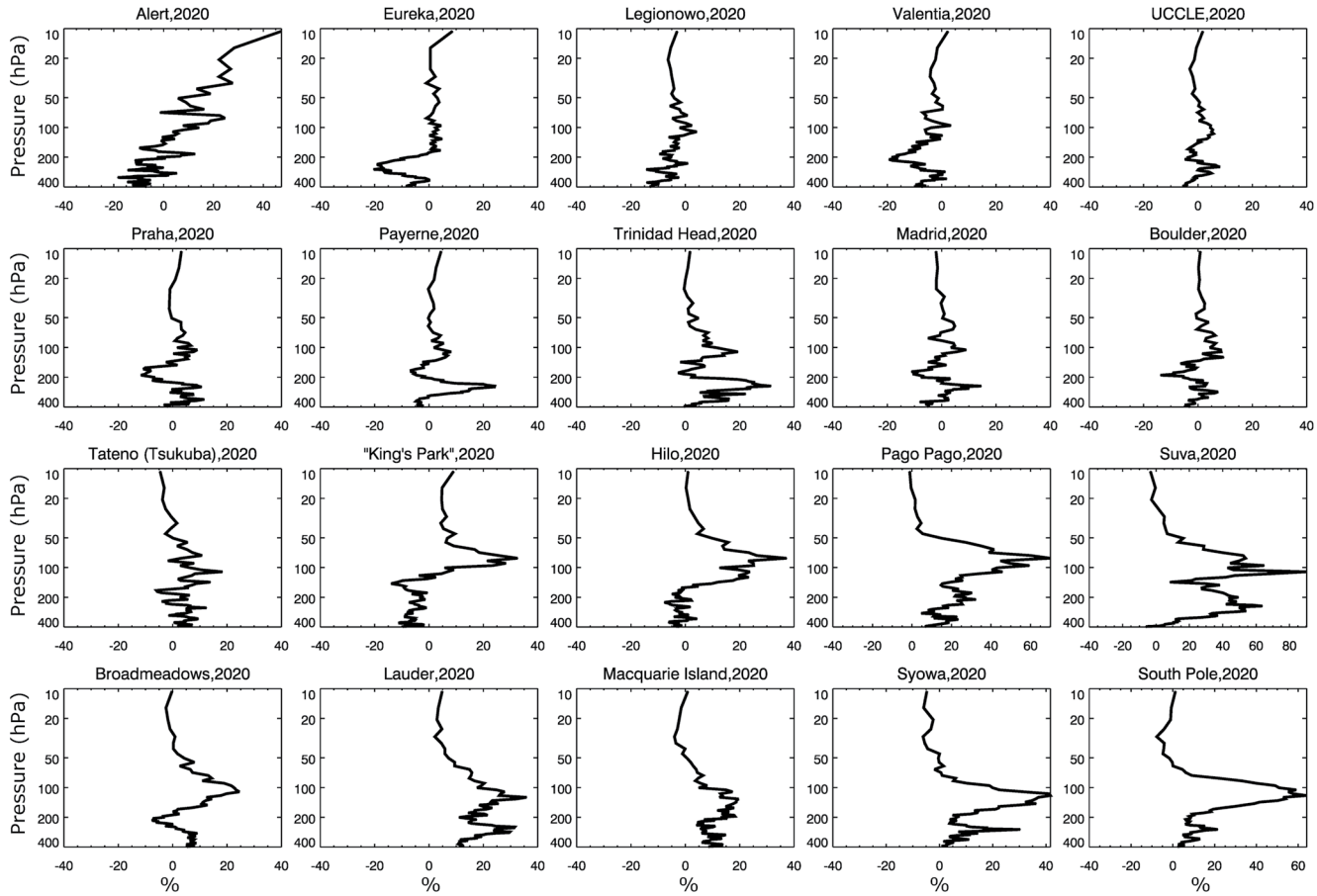

Figure 3. Similar to Figure 2, except median percent bias (GEOS-CF minus ozonesonde divided by ozonesonde). Note, *x*-axis range is generally from −40% to 40% except at Pago Pago, Suva, and South Pole.

most of the stratosphere (Figure 3). While Alert and Eureka are located close to each other in northern Canada (see Figure S2 in Supporting Information S1), the median profiles between 150 and 30 hPa are very different for these two stations. This is attributed to the reduced number of profiles in 2020 for Alert compared to Eureka (17 and 65, respectively, Table 2), since this difference is not present when all profiles from 2018 to 2020 are considered (not shown). In addition, while Suva has the fewest profiles (15; Table 2) and exhibits a similar profile to its closest neighboring site Pago Pago (Figure 2) it has the largest median percent bias of all the profiles (>80% at 100 hPa; Figure 3). Furthermore, at the SH locations (King's Park to South Pole), there is a high bias in GEOS-CF median O_3, most notably between about 200 and 50 hPa (Figures 2 and 3). This is consistent with Stauffer et al. (2019), who assessed the "MERRA2-GMI" product (GEOS with GMI chemistry replayed to MERRA-2 meteorology; Strode et al., 2015) against ozonesondes for the period 1980–2016 and found the subtropical and tropical sonde locations had median percent bias over 20% between 15 and 20 km, and as they note, the median percent biases are large but the O_3 concentrations at these altitudes are low. Stauffer et al. (2019) also present a high bias for the MERRA2-GMI at SH high latitude sites between 10 and 15 km. Here, the differences between GEOS-CF and the SH polar observations at Syowa and South Pole in 2020 are driven by the model not capturing the low O_3 values in this layer of the atmosphere (between about 200 and 50 hPa, 25th percentile, dashed pink line, Figure 2) during austral winter and spring (individual months not shown). Possible reasons for biases in the SH polar regions in 2020 as it relates to polar chemistry are explored later in Sections 5.2 and 7.

Stratospheric O_3 in GEOS-CF also agrees well with SAGE III/ISS solar occultation profiles between 100 and 4.6 hPa for January through December 2020 with correlation coefficients (r) greater than or equal to 0.92 (Figure 4 inset). At higher altitudes, near the stratopause at 1 hPa, the correlation is reduced, $r = 0.61$, with SAGE III/ISS reporting higher concentrations of O_3 than simulated by GEOS-CF (Figure 4). Despite weakly nudging the stratospheric O_3 in GEOS-CF toward the GEOS FP O_3 product which assimilates MLS, the annual

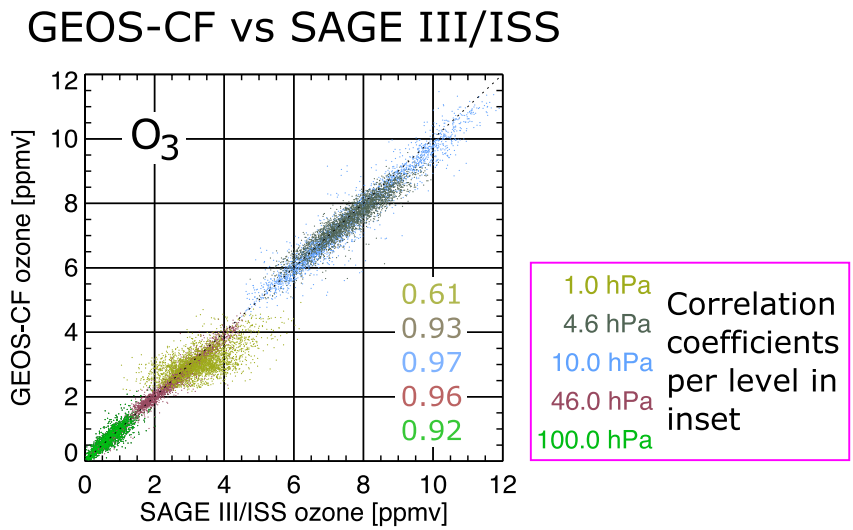

Figure 4. SAGE III/ISS solar occultation O_3 profiles for January–December 2020 interpolated to 5 MLS pressure levels—100, 46, 10, 4.6, 1 hPa—and compared to GEOS-CF O_3.

mean GEOS-CF O_3 is also biased low to MLS O_3 between 5 and 1 hPa globally (Figures 5a–5e). Since H. J. R. Wang et al. (2020) demonstrated very good agreement (<5%) between SAGE III/ISS and MLS in the stratosphere (20–55 km altitude), the difference in upper stratospheric O_3 between GEOS-CF and SAGE III/ISS is likely a deficiency in the model at these altitudes. Previous chemical transport modeling studies have reported negative biases with respect to upper stratospheric/lower mesospheric ozone (e.g., Errera et al., 2019; Eyring et al., 2010; Siskind et al., 2013), and due to the relatively short chemical lifetime of ozone in this region, assimilation was found to not correct for the low bias in the BASCOE system (Skachko et al., 2016). It is very likely that in the upper stratosphere, chemical timescales are shorter than the 3-hr frequency of the ozone nudging in GEOS-CF. The annual zonal mean O_3 distribution for ACE-FTS is greater than GEOS-CF throughout most of the stratosphere, with the maximum difference located near the stratospheric O_3 concentration peak (Figures 5f–5h); the negative bias is expected as ACE-FTS has a known positive bias to coincident MLS profiles (Dupuy et al., 2009; Errera et al., 2019; Sheese et al., 2017, 2022).

As demonstrated by this evaluation against independent observations, GEOS-CF realistically simulates stratospheric O_3 distributions between about 100 and 5 hPa. In the upper stratosphere (5–1 hPa), the disagreement between GEOS-CF simulated O_3 and satellite observations (SAGE III/ISS and MLS) will require further investigation but is likely associated with the extension of stratospheric chemistry up to the mesosphere. The positive bias in GEOS-CF O_3 in the SH polar region between about 200 and 50 hPa present in the comparisons against ozonesondes (Figure 2) and satellite observations by both MLS and ACE-FTS (Figures 5e and 5h) will also be monitored closely.

5.2. Chemical Species Important to Stratospheric O_3 Chemistry

Next, comparisons of the model against satellite observations are presented for stratospheric species that are relevant to polar vortex chemistry and observed by both MLS and ACE-FTS, including two inorganic chlorine species (HCl and ClO), two nitrogen species (HNO_3 and N_2O), and additional nitrogen species only observed by ACE-FTS.

5.2.1. Inorganic Chlorine

Inorganic chlorine in the stratosphere is the result of transport of tropospheric long-lived chlorine compounds, most notably chlorofluorocarbons (e.g., CFC-11 (CCl_3F) and CFC-12 (CCl_2F_2)), chlorinated solvents (e.g., carbon tetrachloride (CCl_4)) and methyl chloride (CH_3Cl). Once in the stratosphere, the long-lived compounds photolyze and react with other chemical species (in the presence of UV) to form reactive chlorine, which through catalytic cycles can lead to loss of stratospheric O_3 (Molina & Rowland, 1974a, 1974b). The CFCs and CCl_4

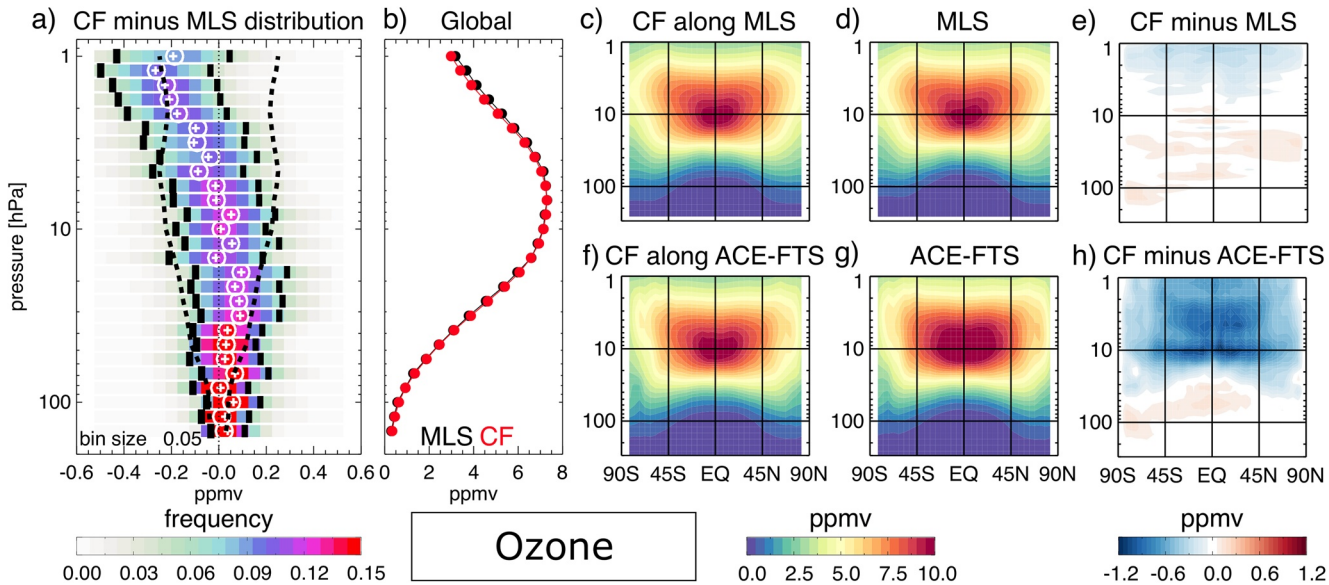

Figure 5. (a) PDF of the differences of GEOS-CF ("CF") O_3 minus MLS O_3 at 27 MLS pressure levels, with mean difference (cross), median difference (open circle), 1σ standard deviation (long dash), and approximate instrument 1σ combined random and systematic uncertainty from the MLS quality document tables (short dash). (b) The mean concentrations for GEOS-CF (red) and MLS (black) at 27 MLS pressure levels from 146.8 to 1.0 hPa. For (a and b), only MLS data within half an hour of the synoptic times (00:00, 6:00, 12:00, 18:00 UTC) are used for January–December 2020. (c and f) Zonal 2020 annual mean O_3 for GEOS-CF co-located to the satellite overpasses, (d and g) the zonal 2020 annual mean O_3 for the satellite and (e and h) the difference of the model minus the satellite for (c–e) MLS and (f–h) ACE-FTS.

are the result of industrial activities and other man-made products which have been phased out following the Montreal Protocol and subsequent amendments (Reimann et al., 2018). CH_3Cl originates mainly from natural sources such as biomass burning emissions, the ocean, and fungi (Keene et al., 1999).

It is critical for the GEOS-CF forecast capabilities of stratospheric O_3 that species such as these are simulated correctly. Several other Cl_y species are observable from space, however, the focus is limited to (a) HCl, a non-ozone-destroying chlorine reservoir and (b) ClO, an active, ozone-depleting chlorine radical (Stolarski & Cicerone, 1974). HCl is abundant in the stratosphere, especially at high altitudes, and as a reservoir species it is relatively inert. Because of the global distribution of these chlorine species, O_3 loss through catalytic cycles can occur throughout the stratosphere; however, this is usually at a slower rate compared to O_3 loss following the conversion of HCl and $ClONO_2$ (another chlorine reservoir) to ClO on PSCs (Solomon et al., 1986) within a sunlit winter-time polar vortex. When polar stratospheric temperatures begin to drop as the vortex forms, the environment becomes favorable for the formation of PSCs. While the maintenance of extremely cold temperatures is more common in the austral winter and spring polar vortex, during the 2020 boreal winter and spring a stable polar vortex led to PSCs which were observed by the OMPS Limb Profiler (LP; DeLand et al., 2020). Within the polar vortex, the heterogeneous chemistry can lead to substantial destruction of stratospheric O_3. This is demonstrated in the snapshot of the NH polar vortex on 29 February 2020 at 22:00 UTC, comparing GEOS-CF simulated concentrations to measurements from a single MLS overpass (Figure 6). As stated in Section 5.1, it is no surprise that the NH O_3 agrees well to MLS in Figure 6a since GEOS-CF at 45 hPa is nudged toward the GEOS FP assimilated product. Presented here is how GEOS-CF simulates the location and chemistry of the vortex; although, GEOS-CF underestimates the observed high values of HCl outside the vortex (Figure 6b) and the highest ClO values within the sunlit portion of the vortex (Figure 6c) as seen by MLS.

Figure 6 is only an example on one pressure level (45 hPa), but it is an accurate representation of the global distribution further investigated in Figures 7 and 8. First, the annual global distribution of HCl from the model is compared against MLS and ACE-FTS profiles of HCl in Figure 7. Throughout the stratosphere, GEOS-CF simulates the vertical gradient of increasing HCl concentrations from the lower stratosphere to upper stratosphere as seen by the satellite measurements. However, the model is biased low compared to the 2020 observations. This holds true at all latitudes except in SH polar region in the lower stratosphere when compared against ACE-FTS measurements where there is a positive difference (100–50 hPa; Figure 7h). The positive bias in ACE-FTS, which is not seen in the annual zonal difference between GEOS-CF and MLS, is likely due to a sampling bias

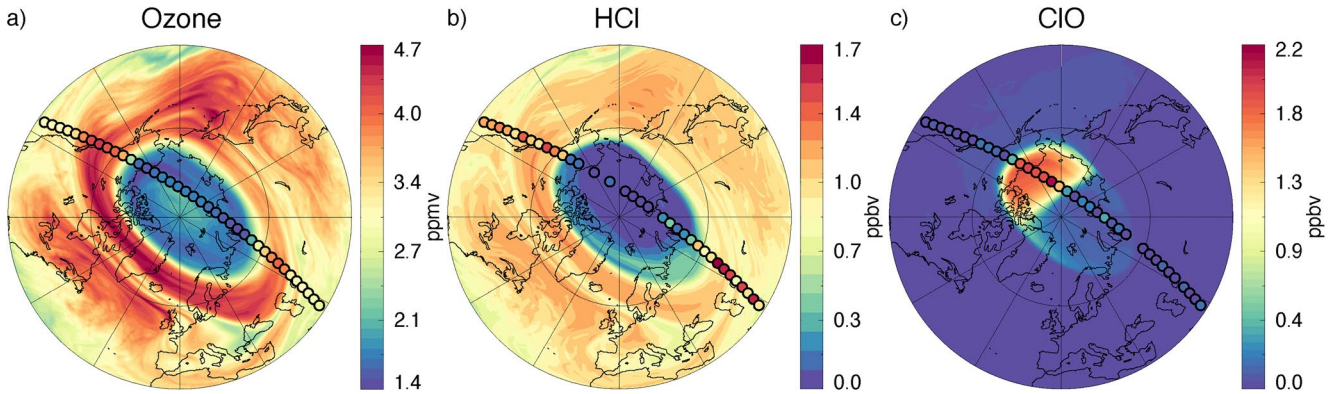

Figure 6. Snapshot of 29 February 2020 at 22:00 UTC for GEOS-CF (map) and a single over-pass of MLS (colored circles; measurements from 21:43 UTC to 22:14 UTC) at 45 hPa for (a) O_3, (b) HCl, and (c) ClO, emphasizing the NH polar vortex chemistry.

by ACE-FTS. The SCISAT orbit is such that ACE-FTS has sunrise measurements south of 60°S only during a few months a year (March, April, July, early August, and November; https://ace.uwaterloo.ca/mission_orbit.php). During July and August, there are positive biases between GEOS-CF and MLS in the SH lower stratosphere (top, Figure S3 in Supporting Information S1), however, there is a large negative bias in late 2020 between GEOS-CF and MLS (Figure S3 in Supporting Information S1) that likely cancels out the mid-year positive biases seen in the SH high latitudes. There is also a bias between ACE-FTS and GEOS-CF $ClONO_2$ (Figure S5 in Supporting Information S1), which may indicate that the Cl_y loading is low in the model.

Second, to look at the vortex chemistry in more detail, the polar distributions of HCl and ClO during February 2020 (NH only; Figures 8a–8d) and August 2020 (SH only; Figures 8e–8h) for three isentropic surfaces (400, 500, and 600 K) are compared for GEOS-CF against MLS. The vortex edge is defined as in Wargan, Weir, et al. (2020) using threshold values of PV scaled by standard static stability ("sPV") selected on isentropic surfaces based on the winter mean sPV gradients in equivalent latitude (Lawrence et al., 2018; Manney et al., 1994). For the model to correctly simulate the O_3 destruction within the vortex, there needs to be an accurate representation of the heterogeneous processes. Within the polar vortexes (NH and SH), concentrations of HCl both observed by MLS and simulated by GEOS-CF decreased compared to outside the vortex (Figure 8); however, GEOS-CF simulated HCl is biased high (low) within the SH (NH) vortex for August 2020 (February 2020) compared to MLS. It is on the PSCs that the chlorine reservoir species are converted to ClO through heterogeneous processes in the presence of sunlight (Figure 8). Within the polar vortexes of 2020, GEOS-CF simulates the increase in ClO abundance within the sunlit portion, although GEOS-CF is biased high with respect to MLS at higher altitudes where there is also a low bias in simulated HCl (600 K, Figures 8d and 8h), likely indicating too much chlorine was activated. Since global distributions of ClO are very low outside of the sunlit portion of the vortex, a comparison on the global scale, similar to Figure 7, was not performed.

5.2.2. Nitrogen Family

Another catalytic cycle for stratospheric O_3 loss is with nitrogen oxides ($NO_x = NO + NO_2$). In the stratosphere, N_2O is the main source for NO and subsequently other nitrogen species collectively referred to as NO_y. We define NO_y as the sum of major reactive nitrogen species: $NO + NO_2 + HNO_3 + ClONO_2 + 2 \times N_2O_5$. A long-lived greenhouse gas, N_2O has natural and anthropogenic sources in the troposphere with no significant sinks until reaching the stratosphere. Once in the stratosphere, N_2O dissociates through photolysis and reaction with excited oxygen atoms to produce NO and is thus a major source of stratospheric NO_y (Crutzen, 1970). During the night time, some NO_2 is converted to N_2O_5, which acts as a reservoir species for NO_x until the sunlight returns. The reaction of ClO with NO_2 forms $ClONO_2$ (Rowland et al., 1976), and $ClONO_2$ is a reservoir species for both reactive chlorine and nitrogen. HNO_3, another nitrogen reservoir, is formed by the reactions of NO_2 with the hydroxyl radical (OH) and through heterogeneous reactions with N_2O_5 and HNO_3 later photolyzes to return OH and NO_2 to the system (Brasseur & Solomon, 2005).

The annual zonal mean distributions of N_2O, NO_x and NO_y in GEOS-CF are compared against measurements from ACE-FTS in Figure 9. While N_2O measurements are available from both MLS and ACE-FTS, profile

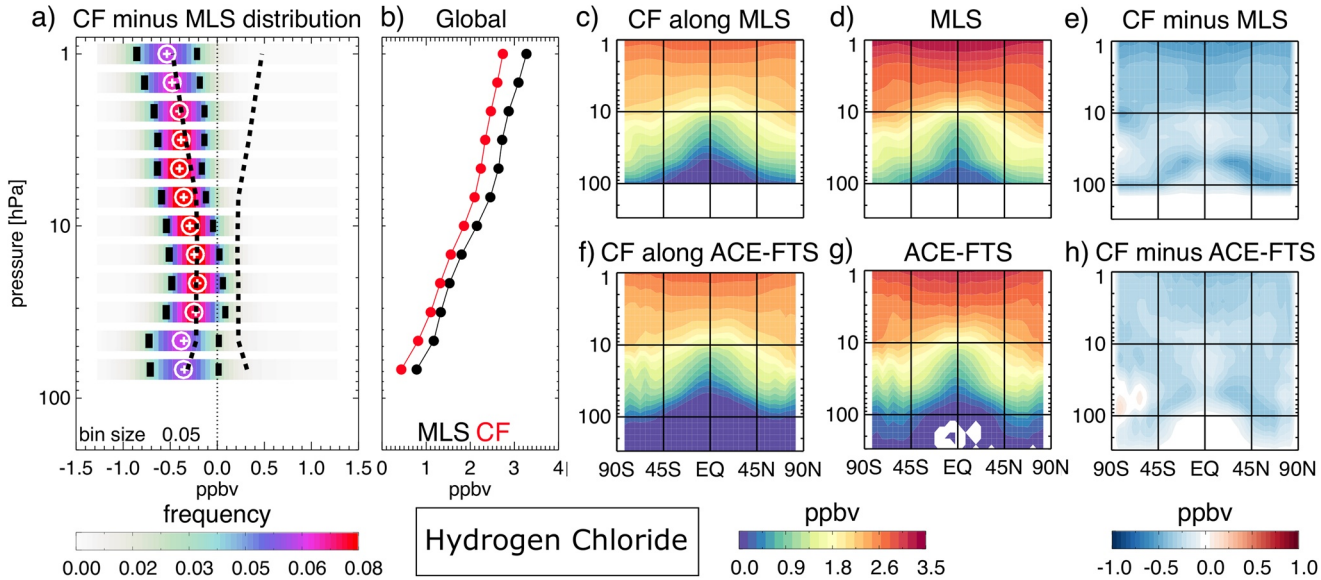

Figure 7. Similar to Figure 5 but for HCl and only MLS data within half an hour of 12:00 UTC for January–December 2020. Negative values from ACE-FTS are colored white (g).

measurements of NO_x are only available from ACE-FTS and there is a known bias in MLS N_2O measurements in the lower stratosphere (Livesey et al., 2021). The expected N_2O distribution based on the known sources and sinks can be clearly seen in Figure 9 (see also Figure S4 in Supporting Information S1 for MLS and ACE-FTS on pressure levels), with the largest concentrations in both the model and the satellite at lower altitudes (closer to tropospheric sources) as well as reaching higher altitudes near the equator because of strong upwelling into the stratosphere over the tropics. At concurrent sampling of GEOS-CF to ACE-FTS measurements, the N_2O spatial patterns for the model and satellite in the stratosphere are consistent, although the model is biased low through much of the stratosphere (isentropic levels up to 1100 K) and biased high in the upper stratosphere (1200–1600 K), particularly in the tropical region (Figure 9; see also from 50 to 5 hPa and 5 to 1 hPa in Figures S4f–S4h of Supporting Information S1 for similar difference patterns in comparison to MLS N_2O).

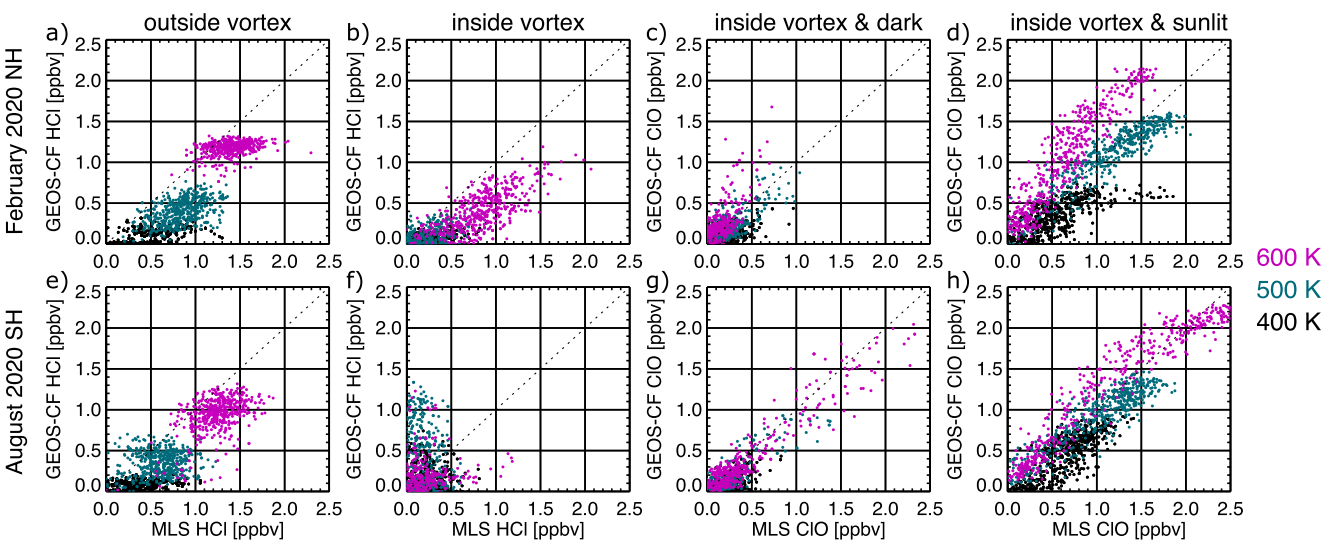

Figure 8. Scatter plots of GEOS-CF (*y*-axis) versus MLS (*x*-axis) for HCl (a–b, e–f) and ClO (c–d, g–h) for NH February 2020 polar vortex (a–d) and SH August 2020 polar vortex (e–h). "Outside vortex" is defined as from 30°N or °S to the vortex edge. The vortex edge is defined as in Wargan, Weir, et al. (2020).

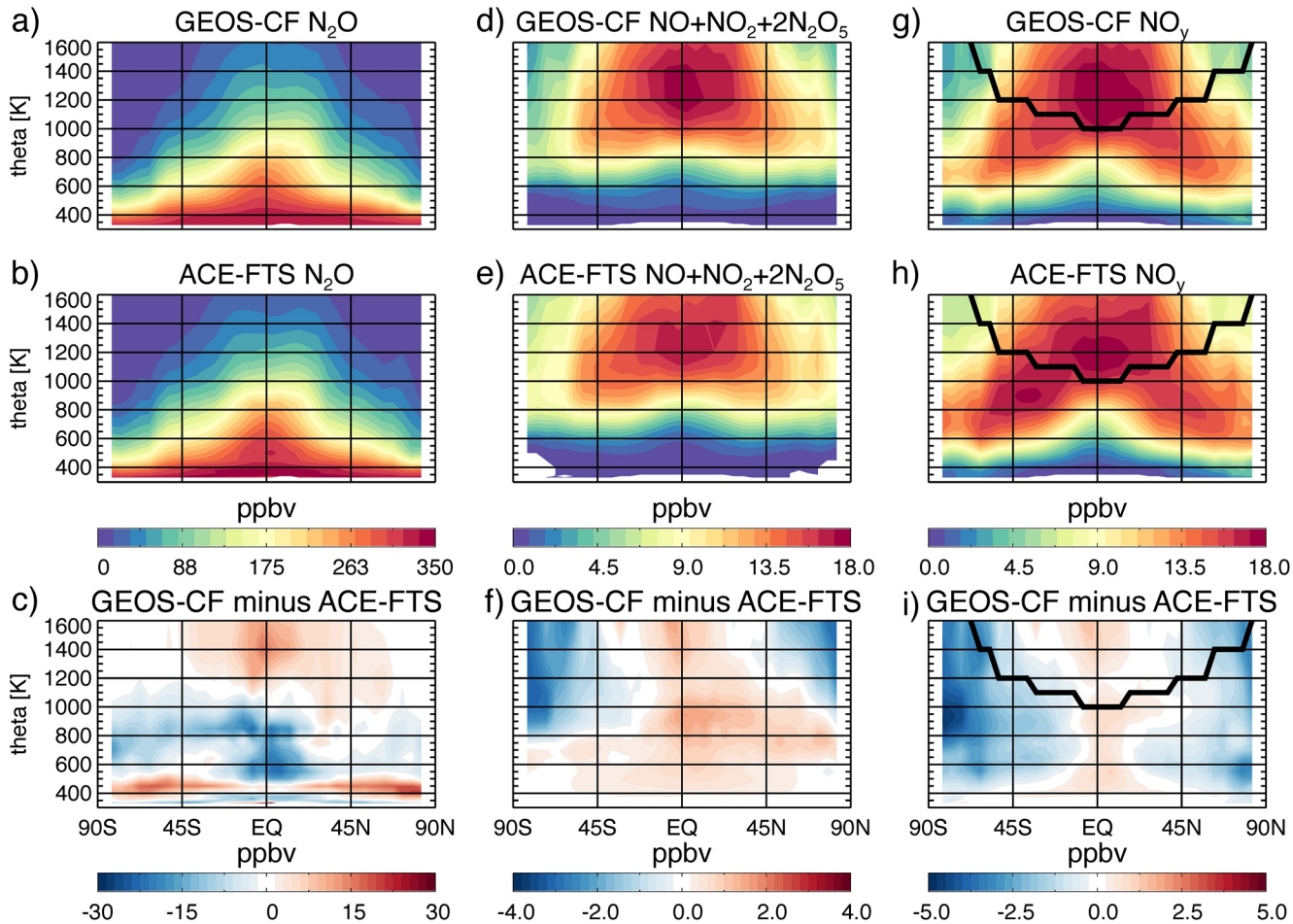

Figure 9. Zonal annual means for GEOS-CF (a, d, and g) and ACE-FTS measurements (b, e, and h) and the difference of GEOS-CF minus ACE-FTS (c, f, and i) for N_2O (a–c), $NO + NO_2 + 2 \times N_2O_5$ ("NO_x^*"; d–f), and NO_y ($NO + NO_2 + HNO_3 + ClONO_2 + 2 \times N_2O_5$; g–i) for isentropic levels from 330 to 1600 K. Note, ACE-FTS does not measure $ClONO_2$ at high altitudes so above the black line $ClONO_2$ missing values were set to zero for the calculation of NO_y (g–i).

To reduce the potential errors because of mismatches around twilight between the GEOS-CF gridpoint and the ACE-FTS measurements, we included N_2O_5 with NO_x as "NO_x^*" to estimate the full diurnal cycle of NO_x in Figures 9d–9f. For both the satellite and GEOS-CF, there is a maximum in NO_x^* (15 and 18 ppbv, respectively) in the tropical upper stratosphere (around 1200–1400 K) and concentrations decrease toward the higher latitudes. Regions of high NO_y extend from the tropics toward lower isentropes and higher latitudes as the mixing ratios of NO_x^* decrease due to the conversion of NO_x into HNO_3 and $ClONO_2$ (Figures 9g and 9h; see also Figure 11 for HNO_3 only distributions and Figure S5 in Supporting Information S1 for NO_y partitioning for ACE-FTS and GEOS-CF).

Since the production of N_2O in the stratosphere is insignificant, it is an ideal tracer for evaluation of model transport that has an anti-correlation with stratospheric age (e.g., Jin et al., 2009; Manney et al., 2009; Ruiz et al., 2021; Strahan et al., 2007). Stratospheric age is the mean time an air parcel has spent in the stratosphere after crossing the tropopause from the troposphere (Waugh, 2009). While the individual nitrogen species in NO_y are not long-lived, together they can be considered as a long-lived tracer. Generally, NO_y mixing ratios increase and N_2O decrease as air "ages" in the stratosphere (see Figure 9); thus, compact relationships form between NO_y and N_2O due to transport and isentropic mixing (e.g., Chang et al., 1996; Koike et al., 2002; Plumb, 2007; Wetzel et al., 2002). Since in the stratosphere air parcels generally move adiabatically, it is useful to explore these relationships using isentropic surfaces (i.e., constant potential temperature). In Figure 10, values of stratospheric NO_y are shown relative to N_2O with colors representing the potential temperature of the individual non-polar points and black for all polar points. Concentrations of N_2O are the highest near the tropospheric sources, seen in both

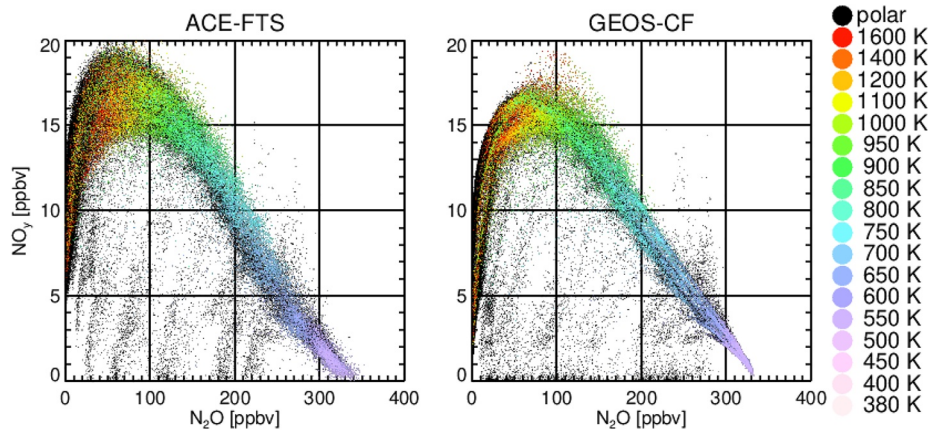

Figure 10. NO_y ($NO + NO_2 + 2N_2O_5 + HNO_3 + ClONO_2$) versus N_2O for ACE-FTS (left) and co-located GEOS-CF (within 1.5 hr, as in Figure 9; right) colored by potential temperature from 380 to 1600 K for latitudes from ±60°, polar observations are black.

ACE-FTS and GEOS-CF at low potential temperature levels. The relationship between N_2O and NO_y is comparable between the satellite and model as air enters the lower stratosphere from the troposphere and ages as it moves upward (to higher potential temperature levels), evidence that GEOS-CF has realistic transport in the lower to middle stratosphere ($N_2O > 100$ ppbv).

However, GEOS-CF does not capture the spread of high values of NO_y (>15 ppbv) observed by ACE-FTS in the stratospherically aged air (i.e., mixing ratios of $N_2O < 100$ ppbv). When the air reaches the upper stratosphere (warm colors in Figure 10, $N_2O < 100$ ppbv) and polar regions (black dots in Figure 10 indicate >|60°|), the tracer-tracer relationship is no longer linear. In the upper stratosphere, chemical processing of NO_y takes place faster than the timescales of the stratospheric transport, as evidenced by the drop off in NO_y as N_2O mixing ratios decrease below 100 ppbv. Similarly, the observed and simulated low values of NO_y and N_2O below the main tracer-tracer curve (black points in Figure 10) suggest that GEOS-CF properly represents the polar vortex mechanisms that remove NO_y from the system until NO_y-rich air from the mid-latitudes replenishes the polar regions after the break-up of the vortex. The NO_y depleting mechanisms that take place within the polar vortex include reversible "denoxification" (removing NO_x from the gas phase) and irreversible "denitrification" (sedimentation of HNO_3-containing PSCs; Salawitch et al., 1989; Toon et al., 1990).

Isolating HNO_3 from NO_y is portrayed in Figure 11. In GEOS-CF, the mid- to high latitude maxima of HNO_3 are simulated correctly in the lower stratosphere between 100 and 10 hPa, where the photochemical lifetime of HNO_3 is long, however the concentrations are not as large as observed by MLS or ACE-FTS (Figures 11c–11h). The variability of the differences, as indicated by the standard deviation (long dash lines) in Figure 11a, peaks between 60 and 15 hPa, which aligns with the increase in the instrument's combined random and systematic uncertainty (short dash lines) and the peak in maximum global HNO_3 concentrations (Figure 11b). Because of the systematic low bias of the model compared to MLS HNO_3, the standard deviation about the mean differences and the uncertainty are offset but otherwise have similar magnitudes. Near the poles, concentrations of HNO_3 decrease (Figures 11c, 11d, 11f, and 11g) through denitrification. The spread of the N_2O:NO_y polar points below the majority of the points in Figure 10 indicates that the model is simulating denitrification similar to ACE-FTS measurements.

In order to inform future model development, we hypothesize some possible reasons for the biases in nitrogen species related to chemistry and emissions that should be considered in future versions of GEOS-CF.

In the polar regions, there are negative differences between ACE-FTS and GEOS-CF NO_x^* in the upper stratosphere and throughout the polar stratosphere for NO_y. This may be linked to missing sources of mesospheric NO_x. One such source is in the thermosphere whereby energetic electrons from galactic cosmic rays react with molecular nitrogen (N_2) to produce atomic nitrogen (N) in either excited $N(^2D)$ or ground $N(^4S)$ state that can then react with molecular oxygen (O_2) or OH to produce NO (e.g., Siskind et al., 1997; Solomon et al., 1982). There is evidence that some of this NO can be transported down into the mesosphere and stratosphere, especially

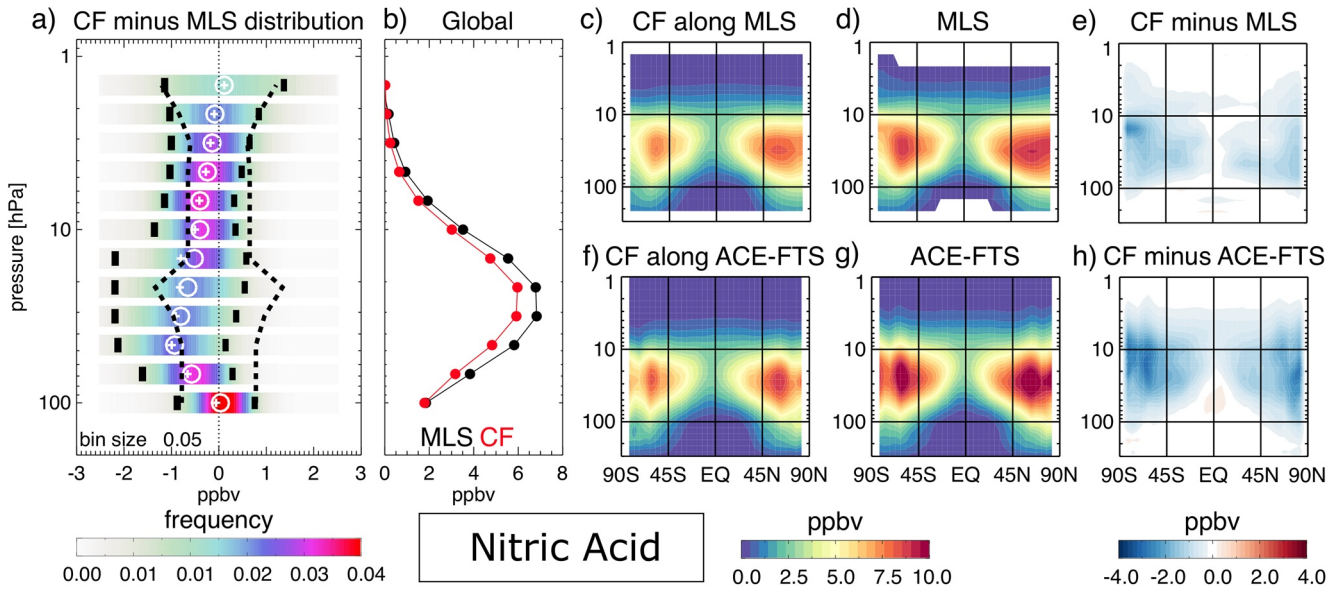

Figure 11. Similar to Figure 7 but for HNO_3.

in the polar regions where there is downwelling in the mesosphere, and concentrations should be higher as it is not photochemically destroyed during polar night (Funke et al., 2005; Randall et al., 2005, 2007). This missing source from galactic cosmic rays has been identified in another modeling study to explain some of the discrepancies in chlorine and nitrogen species associated with the SH winter and spring polar vortex when compared against satellite observations (Grooß et al., 2018). Sources of mesospheric NO_x are not represented in the GEOS-CF system and may be further confounded by the extension of stratospheric chemistry into the mesosphere in GEOS-CF (see Section 2). Furthermore, when each month is assessed individually, from April 2020 to August 2020, the SH stratospheric low HNO_3 bias decreases in the same region as the high bias in HCl (Figure S3 in Supporting Information S1) while the biases in both HCl and HNO_3 increase along the vortex edge instead of in the vortex center during winter time in keeping with the findings of Grooß et al. (2018) for HCl. A future version of GEOS-CF may benefit from upper-boundary emission sources representing the solar and galactic high energy particles as diagnosed by Grooß et al. (2018).

In the equatorial stratosphere there is a positive bias in NO_x^* and NO_y between the model and ACE-FTS (Figures 9f and 9i). As stated in Keller et al. (2021), GEOS-CF uses the unadjusted lightning parameterization (described in Murray et al. [2012]) which leads to higher lightning NO_x in the tropics. However, this is likely a very small contribution to the positive difference seen in the equatorial region between observations and model in Figure 9. Another theory is the positive bias of N_2O above the large negative bias in the tropics (Figure 9c) may indicate that the vertical transport is too fast, however the model generally captures the observed distributions of nitrogen-containing species (Figures 9a and 9b) and the N_2O to NO_y relationship in the lower to mid-stratosphere (Figure 10), both indicating that GEOS-CF correctly captures the large-scale transport pathways (Holton, 1986; Mahlman et al., 1986). Instead of transport, the biases may be due to chemistry. Higher in the equatorial stratosphere, the GEOS-CF maximum in NO_x^* is larger in magnitude and extends to higher potential temperature surfaces than observed by ACE-FTS (Figures 9d and 9e). The positive bias in GEOS-CF NO_x^* is in a similar location as the positive bias in N_2O. With the increased available N_2O, production of NO_x^* may be greater in the upper stratosphere than is observed. Also, the conversion to other nitrogen species, such as HNO_3, may be too slow, as indicated by NO_y partitioning (Figure S5 in Supporting Information S1).

6. Evaluation of Stratospheric O_3 Forecast Capability

In Section 5, the state of the stratospheric composition for GEOS-CF when the model is constrained by observed meteorology was characterized. In this section, a few case studies explore the skill of the GEOS-CF model during the 5-day forecasts when the meteorology and chemistry are free-running. First, the evaluation of 5-day forecasts

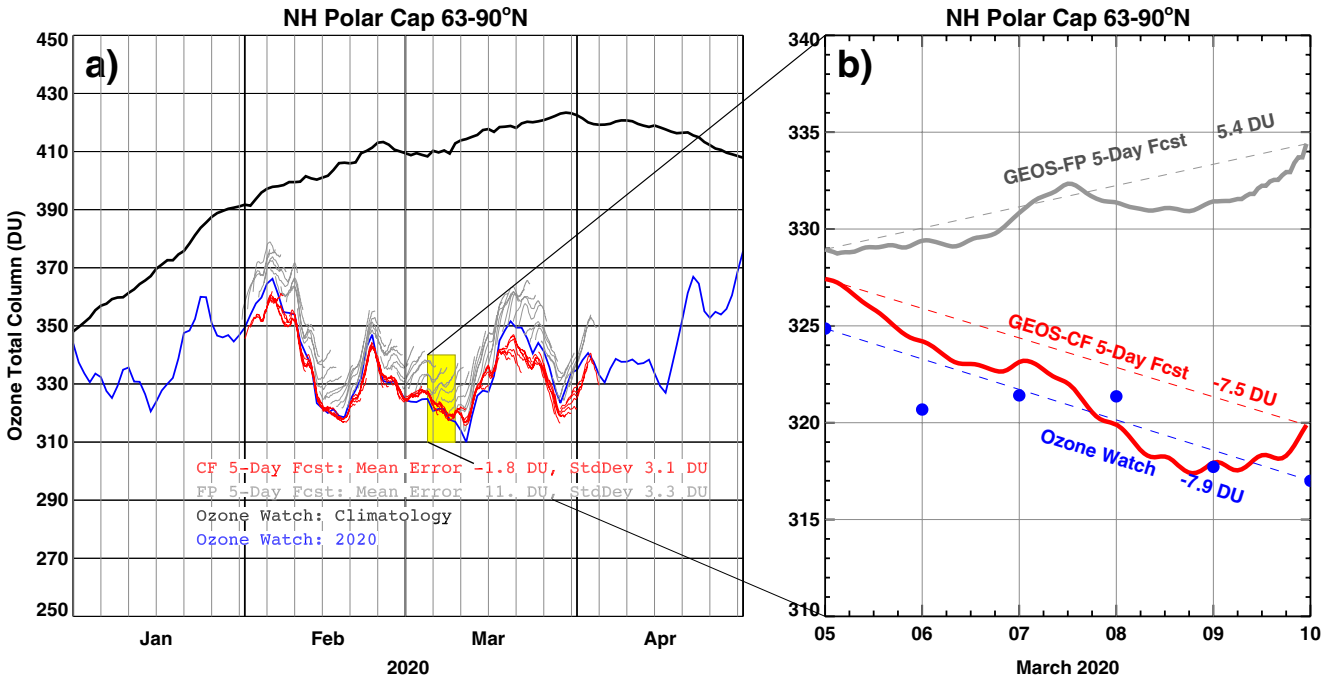

Figure 12. Total column O_3 (DU) for the NH Polar Cap region (63°–90°N) from GEOS-CF 5-day forecast trajectories (red), GEOS FP 5-day forecast trajectories (gray), Ozone Watch analysis (blue), and Ozone Watch 1979–2020 climatology (black) (a) from January to April 2020 and (b) from 5 March to 10 March 2020 for forecast initialized 12:00 UTC 5 March 2020. (a) The thick vertical lines denote the first day of each month, while the light vertical lines denote 5-day intervals starting from 1 January 2020. The yellow box indicates the period of the case study in (b). (b) Date labels correspond to mid-point in the day (12:00 UTC).

for the NH and SH anomalous polar events using GEOS-CF and GEOS FP against the NASA Ozone Watch merged satellite product is presented. The year 2020 highlighted some aspects of stratospheric O_3 interannual variability which occur because of both atmospheric dynamics and chemistry. In particular, during the boreal winter to spring, the relatively undisturbed stratosphere allowed the NH polar vortex and associated anomalously low polar O_3 to persist (e.g., Dameris et al., 2021; Inness et al., 2020; Lawrence et al., 2020; Manney et al., 2020; Wohltmann et al., 2020). A similar situation existed in the 2020 austral late winter and spring, where, as will be shown below the strongly zonal stratospheric winds allowed the SH ozone hole to extend longer than normal (Lecouffe et al., 2022). Thus, in both time periods, polar O_3 column values were generally far below their climatological values, highlighting the need during these times for O_3 chemistry forecasts based on full stratospheric O_3 chemistry (e.g., GEOS-CF) rather than parameterized chemistry (e.g., GEOS FP) which can be based on average production and loss rates or an O_3 climatology. GEOS-CF forecasts are first described for the 2020 NH anomalous event for the total O_3 column in the 63°–90°N polar cap (Section 6.1), followed by forecasts for the area of the 2020 SH ozone hole size as measured by the total O_3 column less than 220 DU (Section 6.2).

Another application of the GEOS-CF forecasts is the ability to provide the air quality community with realistic 5-day forecasts of stratospheric intrusion events, when stratospheric O_3-rich air is irreversibly mixed into the troposphere, which can lead to O_3 air quality exceedances events especially at high altitude locations. This new capability is highlighted in Section 6.3 (see also Duncan et al. [2021]).

6.1. NH Spring 2020 Polar Ozone Anomaly

Figure 12 depicts the record low NH polar cap O_3 during January–April 2020 (blue curve compared to black curve, Figure 12a; e.g., Inness et al., 2020; Lawrence et al., 2020; Manney et al., 2020) with the average value for March being approximately 75 DU (20%) below climatology. During this time, the 5-day GEOS FP forecast trajectories (gray curves) tended toward the higher climatological values (e.g., for March is on the order of 400–450 DU; Feng et al., 2021), as expected with simplified chemistry. On the other hand, the corresponding GEOS-CF trajectories (red curves) remained consistent with the future GEOS-CF initial values, as the sophisticated GEOS-Chem chemistry is able to simulate a more realistic atmosphere. The smaller GEOS-CF mean

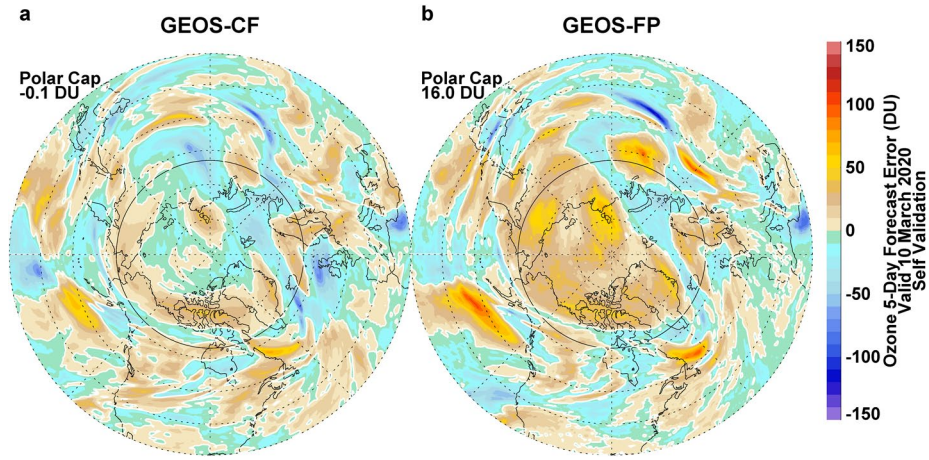

Figure 13. Total O_3 forecast error (DU) for 10 March 2020 calculated by the 5-day forecast initialized on 5 March 2020 at 12:00 UTC minus the analysis (date the forecast is valid) from (a) GEOS-CF and (b) GEOS FP. Solid black circle indicates the 63°N latitude for the polar cap region of interest.

5-day bias (with respect to the concurrent GEOS-CF replay) for February and March period, −1.8 DU, compared to the GEOS FP bias (with respect to concurrent GEOS FP analyses), 11 DU, reflects this tendency (see inset, Figure 12a). The GEOS-CF mean behavior consistently tracked closely to the independently analyzed Ozone Watch values (blue contour). The closeness of the GEOS-CF and GEOS FP 5-day forecast's standard deviation of the error, 3.1 and 3.3 DU respectively (see inset, Figure 12a), indicate that both systems realistically captured the day-to-day dynamically induced variations of polar cap O_3.

As a specific example, the GEOS-CF and GEOS FP forecast trajectories, initialized on 5 March 2020, evolved in different directions (Figure 12b). Since GEOS-CF is nudged toward the GEOS FP O_3, the forecasts start at a similar place; however, GEOS-CF and GEOS FP forecasted changes of −7.5 and 5.4 DU, respectively, over the 5-days. In this example, the GEOS-CF predicted polar cap O_3 decrease agreed well with the Ozone Watch analyzed change of −7.9 DU. Furthermore, a hemispheric view of the 5-day forecast error for the 10 March 2020 (Figure 13) reveals a substantial increase over most of the polar cap in GEOS FP compared to the more random error pattern found in GEOS-CF. In addition to the errors in the polar cap, GEOS FP NH middle latitude O_3 column errors often peak higher than the corresponding GEOS-CF errors (Figure 13, red values).

6.2. SH 2020 Ozone Hole Area

As demonstrated in Figure 14, the distinctive, long duration, 2020 ozone hole (defined where TCO < 220 DU; blue line) kept its area larger than the climatological average (black line) from August until after November. The anomalous polar vortex conditions again push past the limits of the GEOS FP O_3 forecasts with simple chemistry, as in the 2020 NH spring. Forecasting the ozone hole area during the development of the SH ozone hole in August proved difficult for both GEOS-CF and GEOS FP; since weak gradients near the 220 DU value exist at this time, it makes exact determination of the area difficult, which may influence the analysis uncertainty at this stage. In addition, the sunless August polar region limits coverage of solar backscatter satellite O_3 observations and therefore less observational constraints on the models' analyzed O_3. However, by the middle of September, the ozone hole area determined from the GEOS FP initial conditions (GEOS FP analysis, corresponding to the start of each gray line) and the GEOS-CF 5-day forecast trajectories (start of each red line) agreed well with the O_3 Watch 2020 values.

As expected, the GEOS FP 5-day forecasts tended toward a smaller ozone hole area, more characteristic of the climatological ozone hole area (black line, Figure 14; see also Figure 8 of Nielsen et al. [2017]). Over the 4-month period and using self-validation (in units of 10^6 km^2), the GEOS FP fifth-day forecast bias (−2.45; see inset Figure 14) greatly exceeded in magnitude the GEOS-CF forecast bias (−0.13), and the GEOS FP error standard deviation (2.13) also exceeded that of GEOS-CF (0.64). Thus, despite not simulating the ozone hole area

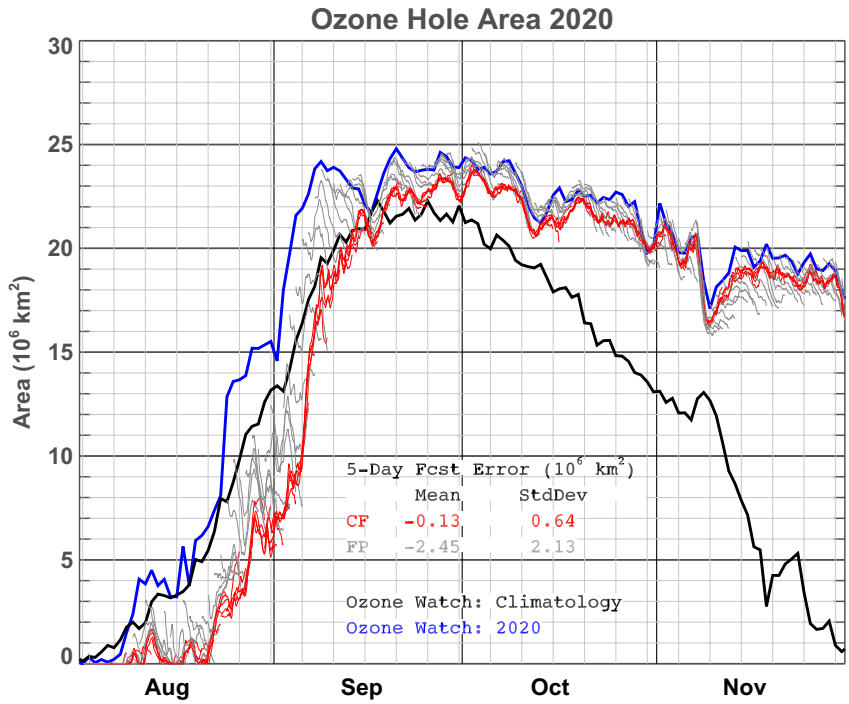

Figure 14. Similar to Figure 12a except for ozone hole area (10^6 km^2) from August to November 2020, with the 5-day intervals starting from 1 August 2020.

consistent with Ozone Watch at the onset in August, during the SH ozone hole of 2020, GEOS-CF successfully forecasted changes in the ozone hole area out to 5-days.

6.3. Forecast Capability for Stratospheric Intrusions

Stratospheric intrusions occur when the tropopause—the boundary between the stratosphere and troposphere—wraps around the jet core, bringing stratospheric air down toward the surface. This folding of the tropopause is generally associated with upper-tropospheric level troughs and cut-off lows. These synoptic weather patterns occur year round, however the tropopause folding events are of interest to air quality managers especially in the spring and early summer (March through June). During this time of year there is a maximum in O_3 in the lower stratosphere which is drawn down within a fold and the photochemical production of O_3 at the surface is not yet the dominant source of O_3 leading to air quality standard exceedances. Ott et al. (2016) and Knowland et al. (2017) both demonstrated that the GEOS model run at horizontal resolutions of 50 km or less with O_3 data assimilation can represent stratospheric intrusions which are linked with ground-level O_3 enhancements, however the tropospheric O_3 is biased from the simplified chemistry used in the GEOS forecast and reanalysis products prior to the inclusion of GEOS-Chem in the GEOS-CF system.

Tropospheric O_3 lidars have a demonstrated record of successfully measuring stratospheric intrusions (e.g., Kuang et al., 2012, 2017; Langford et al., 2009). Here one example of a large stratospheric intrusion event forecasted in near-real time by GEOS-CF to pass over NASA JPL's TMF (Figure 15) on 13 June 2020 as captured by TMTOL (Figure 16a) is examined. Five days in advance, the GEOS-CF indicated a potential O_3 enhancement above TMF that is likely of stratospheric origin; above 6 km O_3 concentrations exceeded 150 ppbv, the value commonly used to define the chemical tropopause (Prather et al., 2001) (Figure 15a). This feature was then present in each of the 5-day forecasts at decreasing lag times (Figures 15b–15e), indicating a high likelihood that it is a dynamic event and will be realized. At the location of TMF, GEOS-CF simulates both the high levels of stratospheric O_3 and the photochemically produced O_3 enhancement transported from Los Angeles basin up to TMF (high levels of O_3 near the 2,000 m altitude; Figure 15).

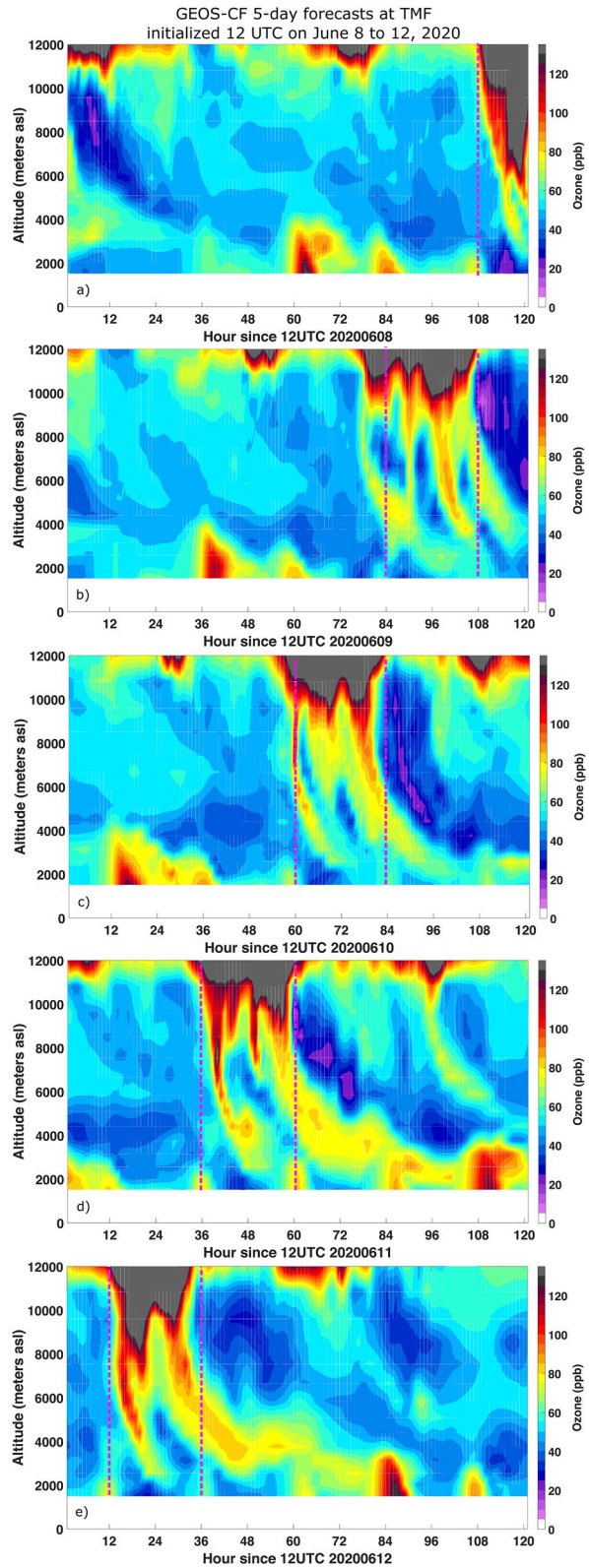

Figure 15. GEOS-CF 5-day (120 hr) O_3 forecasts for grid box closest to Table Mountain Facility (TMF) (34.25°N, 117.75°W) initialized at 12:00 UTC on (a) 8 June 2020, (b) 9 June 2020, (c) 10 June 2020, (d) 11 June 2020, and (e) 12 June 2020. The GEOS-CF O_3 on 23 pressure levels from 1,000 to 10 hPa are interpolated to altitude in meters asl for comparison to TMF observations (see Figure 16). Vertical pink dashed lines indicate the 24-hr period of 13 June 2020 in each of the forecasts.

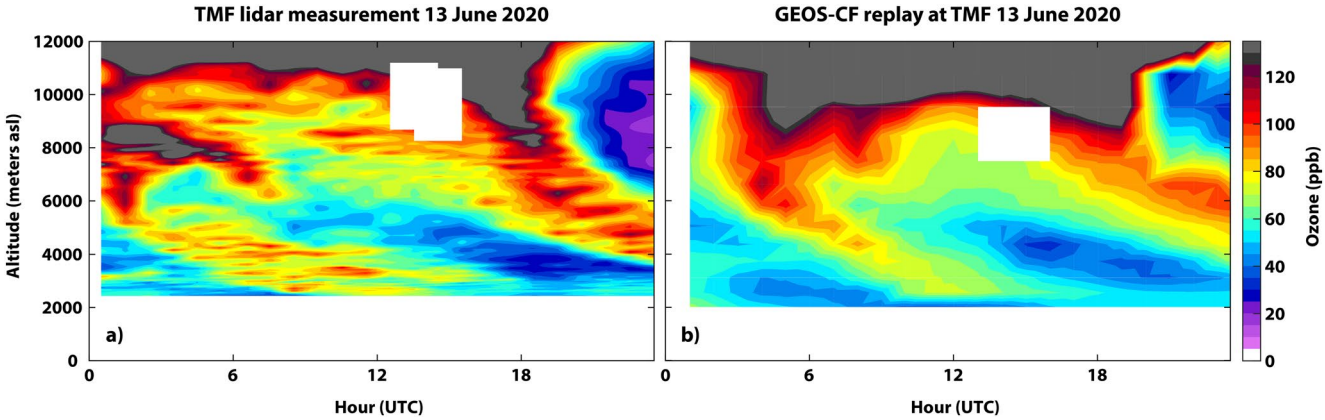

Figure 16. O_3 curtains on 13 June 2020 from (a) the TMTOL measurements (30 m vertical resolution) and (b) similar to Figure 15 except GEOS-CF replay O_3 for the hours of TMTOL operation. The white areas are where high quality lidar data was unavailable. For comparison, the co-located model data are also removed and indicated as white space.

On 13 June 2020, the TMTOL operated throughout the day (Figure 16a). The GEOS-CF replay output (Figure 16b; originally on pressure levels and converted to altitude) simulates the two O_3 tongues around the time of enhancements seen by the TMTOL. While there are differences in the extent and timing of the O_3-rich air descending into the troposphere, this example highlights the strengths of the GEOS-CF's coupled stratosphere-troposphere chemistry in its ability to forecast the impact of stratospheric composition on tropospheric air quality.

7. Conclusions

NASA's GEOS Composition Forecast system (GEOS-CF; Keller et al., 2021) provides near real-time estimates of recent atmospheric composition with daily 5-day forecasts at high spatial resolution (0.25° latitude × 0.25° longitude up to the lower mesosphere) and high temporal frequency (3D at hourly and 3-hourly intervals). GEOS-CF products are used to support ground-based, balloon, and satellite-based instrument teams, as well as field and aircraft campaigns that measure trace gases in the troposphere and the stratosphere. Specifically, for surface air quality, it is important that GEOS-CF simulates the stratosphere to troposphere transport as stratospheric O_3 can be transported to the surface and impact surface air quality. Based on this new capability from the GEOS forecast models, GEOS-CF is used in a daily tailored email alert system for the TOLNet operators. Furthermore, with the meteorology and composition on an identical grid, this makes it ideal to support satellite observations that need a priori information from a model for the trace gas retrievals or to diagnose stratospheric from tropospheric air masses. Instrument teams, such as for TEMPO (Tropospheric Emissions: Monitoring of Pollution; Zoogman et al., 2017), will benefit from near-real time prior information provided by GEOS-CF for their satellite retrievals.

This study focused on concentrations of stratospheric O_3 and chemical species which play a role directly or indirectly in stratospheric O_3 chemistry. Not all chemical species simulated by GEOS-CF have observations available for validation, however an extensive list of chemical species on 3D model output are made available to the public for research purposes (Knowland et al., 2022). Comparisons against independent observations focused on the year 2020, allowing several months for the stratosphere to stabilize after updates were made to the GEOS-Chem UCX module on 31 July 2019 for improved stratospheric chemistry and composition in the GEOS-CF product. Observation suite included ozonesondes and satellites (namely ACE-FTS, MLS, and SAGE III/ISS) to provide a general overview of the global state of the GEOS-CF stratospheric composition. Since the GEOS-CF replay O_3 is constrained by observations by nudging toward the GEOS FP assimilated O_3 product, it is expected to agree well with independent observations in the stratosphere. The median O_3 simulated in GEOS-CF colocated with 20 ozonesonde locations agrees well in the stratosphere (400–10 hPa), and the median percent bias is within ±20% through most of the stratosphere. GEOS-CF correlates well with SAGE III/ISS observations ($r > 0.92$) between 100 and 4.6 hPa, but near the stratopause the relationships tend to break down ($r = 0.61$ at 1 hPa). Overall, the spatial patterns of the GEOS-CF simulated concentrations agree well with MLS and ACE-FTS for chlorine (HCl and ClO) and nitrogen (HNO_3; ACE-FTS only for N_2O, NO_x^*, and NO_y) species.

With the inclusion of the complex chemistry in GEOS-CF, during extremely low column O_3 events, such as occurred within the NH and SH polar vortexes of 2020, the GEOS-CF forecasts can realistically predict key features of stratospheric O_3 variability. GEOS-CF captures the dynamical and chemical environments of the polar vortexes since heterogeneous reactions on PSCs are represented in the GEOS-Chem UCX mechanism. Specifically, it simulates low concentrations of HCl within the polar vortex and high concentrations of ClO within the sunlit portion, which leads to the destruction of O_3 within the vortex. While biases can exist in the initial conditions and forecasts, in situations where the bias is unimportant or can be corrected, GEOS-CF forecasts should prove especially useful. Future development, as more years of GEOS-CF output become available, will focus on better characterizing this bias. There is also the potential for longer, 10-day, O_3 forecasts pending future demand.

One new development from GMAO is the expanded GEOS DAS to multi-constituent assimilation ("CoDAS"). Demonstrated by Wargan, Weir, et al. (2020), the assimilation of stratospheric O_3, HCl, H_2O, and N_2O from MLS with a stratospheric chemistry model can offer a more realistic representation of important species related to stratospheric O_3 recovery, in particular within the polar vortex. Stratospheric H_2O in reanalysis products are historically poor (Davis et al., 2017), and without an observational constraint on H_2O above the tropopause, the GEOS-CF stratospheric water vapor is also biased compared to independent observations from MLS and ACE-FTS (Figure S6 in Supporting Information S1). In addition to HNO_3, water vapor is important for PSCs and other heterogeneous processes. Future developments for the GEOS-CF system include incorporating the CoDAS system to constrain both tropospheric and stratospheric constituents. The first test will include the assimilation of stratospheric O_3 to remove the need for the O_3 nudging technique. With the assimilation of satellite-retrieved H_2O and other stratospheric species, GEOS-CF would likely improve on the spatial distribution of these and other related chemical species globally, and especially in and around a polar vortex.

Data Availability Statement

All GEOS-CF model output is centrally stored at the NASA Center for Climate Simulation (NCCS). Public access to these archives is provided by the GMAO at https://gmao.gsfc.nasa.gov/weather_prediction/GEOS-CF/data_access through model output access tools including OPeNDAP and Hypertext Transfer Protocol (HTTP). The SBUV merged data set is available from https://acd-ext.gsfc.nasa.gov/Data_services/merged/index.html, OMI "TOMS-like" level 3 gridded product (Bhartia, 2012) available from https://disc.gsfc.nasa.gov/datasets/OMTO3d_003/summary, OzoneWatch is available from https://ozonewatch.gsfc.nasa.gov/, SAGE III-ISS data is available from the NASA Langley Research Center Atmospheric Sciences Data center (https://eosweb.larc.nasa.gov/project/SAGE%20III-ISS), OMI and MLS data is available at https://disc.gsfc.nasa.gov/, and TOLNet available from https://www-air.larc.nasa.gov/missions/TOLNet/data.html. The ozonesondes are available from http://www.woudc.org and https://gml.noaa.gov/aftp/data/ozwv/Ozonesonde/. ACE-FTS measurements are available, following registration, from http://www.ace.uwaterloo.ca/data.php, with the data quality information available at https://dataverse.scholarsportal.info/dataset.xhtml?persistentId=doi:10.5683/SP2/BC4ATC.

Acknowledgments
K. E. Knowland, C. A. Keller, P. A. Wales, K. Wargan, L. Coy, L. E. Ott, S. Pawson acknowledge support by the NASA Modeling, Analysis and Prediction (MAP) Program (Project manager David Considine). Support for E. Fleming, J. Liu, Q. Liang was provided by the CCM work package funded by the NASA MAP. M. S. Johnson was funded for this work by the NASA Tropospheric Composition Program as part of the TOLNet Science Team. The research carried out at JPL, California Institute of Technology, was performed under a contract with the National Aeronautics and Space Administration (80NM0018D0004). The Atmospheric Chemistry Experiment is a Canadian-led mission mainly supported by the CSA. The authors acknowledge Sterling Spangler for technical assistance to produce Figure S1 in Supporting Information S1. Resources supporting the GEOS-CF and GEOS CCM model simulations were provided by the NASA High-End Computing (HEC) Program through the NASA Center for Climate Simulation (NCCS) at Goddard Space Flight Center. The authors thank the two anonymous reviewers for their careful and thorough read of the manuscript and their helpful suggestions.

References

Bak, J., Liu, X., Kim, J.-H., Haffner, D. P., Chance, K., Yang, K., & Sun, K. (2017). Characterization and correction of OMPS nadir mapper measurements for ozone profile retrievals. *Atmospheric Measurement Techniques*, *10*(11), 4373–4388. https://doi.org/10.5194/amt-10-4373-2017

Bernath, P. F. (2017). The Atmospheric Chemistry Experiment (ACE). *Journal of Quantitative Spectroscopy and Radiative Transfer*, *186*, 3–16. (Satellite Remote Sensing and Spectroscopy: Joint ACE-Odin Meeting, October 2015). https://doi.org/10.1016/j.jqsrt.2016.04.006

Bernath, P. F., McElroy, C. T., Abrams, M. C., Boone, C. D., Butler, M., Camy-Peyret, C., et al. (2005). Atmospheric Chemistry Experiment (ACE): Mission overview. *Geophysical Research Letters*, *32*(15), L15S01. https://doi.org/10.1029/2005GL022386

Bey, I., Jacob, D. J., Yantosca, R. M., Logan, J. A., Field, B. D., Fiore, A. M., et al. (2001). Global modeling of tropospheric chemistry with assimilated meteorology: Model description and evaluation. *Journal of Geophysical Research*, *106*(D19), 23073–23095. https://doi.org/10.1029/2001JD000807

Bhartia, P. K. (2012). *OMI/Aura TOMS-Like Ozone, Aerosol Index, Cloud Radiance Fraction L3 1 day 1 degree × 1 degree V3*. NASA Goddard Space Flight Center, Goddard Earth Sciences Data and Information Services Center (GES DISC). https://doi.org/10.5067/Aura/OMI/DATA3001

Bhartia, P. K., & McPeters, R. D. (2018). The discovery of the Antarctic Ozone Hole. *Comptes Rendus Geoscience*, *350*(7), 335–340. https://doi.org/10.1016/j.crte.2018.04.006

Boone, C. D., Bernath, P. F., Cok, D., Jones, S. C., & Steffen, J. (2020). Version 4 retrievals for the atmospheric chemistry experiment Fourier transform spectrometer (ACE-FTS) and imagers. *Journal of Quantitative Spectroscopy and Radiative Transfer*, *247*, 106939. https://doi.org/10.1016/j.jqsrt.2020.106939

Brasseur, G. P., & Solomon, S. (2005). *Aeronomy of the middle atmosphere: Chemistry and physics of the stratosphere and mesosphere* (Vol. 32). Springer Science & Business Media.

Bucsela, E. J., Krotkov, N. A., Celarier, E. A., Lamsal, L. N., Swartz, W. H., Bhartia, P. K., et al. (2013). A new stratospheric and tropospheric NO_2 retrieval algorithm for nadir-viewing satellite instruments: Applications to OMI. *Atmospheric Measurement Techniques*, *6*(10), 2607–2626. https://doi.org/10.5194/amt-6-2607-2013

Burkholder, J. B., Sander, S. P., Abbatt, J. P. D., Barker, J. R., Huie, R. E., Kolb, C. E., et al. (2015). *Chemical kinetics and photochemical data for use in atmospheric studies, evaluation No. 18, JPL Publication 15-10*. Jet Propulsion Laboratory. Retrieved from http://jpldataeval.jpl.nasa.gov

Carpenter, L. J., & Daniel, J. S. (2018). *Scenarios and information for policymakers, chapter 6 in scientific assessment of ozone depletion: 2018. Global Ozone Research and Monitoring Project — Report No. 58*. Retrieved from https://csl.noaa.gov/assessments/ozone/2018/downloads/Chapter6_2018OzoneAssessment.pdf

Carslaw, K. S., Peter, T., & Clegg, S. L. (1997). Modeling the composition of liquid stratospheric aerosols. *Reviews of Geophysics*, *35*(2), 125–154. https://doi.org/10.1029/97RG00078

Chang, A. Y., Salawitch, R. J., Michelsen, H. A., Gunson, M. R., Abrams, M. C., Zander, R., et al. (1996). A comparison of measurements from ATMOS and instruments aboard the ER-2 aircraft: Tracers of atmospheric transport. *Geophysical Research Letters*, *23*(17), 2389–2392. https://doi.org/10.1029/96GL01677

Chen, Q., Schmidt, J. A., Shah, V., Jaeglé, L., Sherwen, T., & Alexander, B. (2017). Sulfate production by reactive bromine: Implications for the global sulfur and reactive bromine budgets. *Geophysical Research Letters*, *44*(13), 7069–7078. https://doi.org/10.1002/2017GL073812

Chouza, F., Leblanc, T., Brewer, M., & Wang, P. (2019). Upgrade and automation of the JPL Table Mountain Facility tropospheric ozone lidar (TMTOL) for near-ground ozone profiling and satellite validation. *Atmospheric Measurement Techniques*, *12*(1), 569–583. https://doi.org/10.5194/amt-12-569-2019

Cisewski, M., Zawodny, J., Gasbarre, J., Eckman, R., Topiwala, N., Rodriguez-Alvarez, O., et al. (2014). The Stratospheric Aerosol and Gas Experiment (SAGE III) on the International Space Station (ISS) Mission. In *Proceedings of SPIE. Sensors, Systems, and Next-Generation Satellites XVIII* (Vol. 9241, p. 924107). International Society for Optics and Photonics. https://doi.org/10.1117/12.2073131

Clark, H., Bennouna, Y., Tsivlidou, M., Wolff, P., Sauvage, B., Barret, B., et al. (2021). The effects of the COVID-19 lockdowns on the composition of the troposphere as seen by In-service Aircraft for a Global Observing System (IAGOS) at Frankfurt. *Atmospheric Chemistry and Physics*, *21*(21), 16237–16256. https://doi.org/10.5194/acp-21-16237-2021

Collins, M., Knutti, R., Arblaster, J., Dufresne, J.-L., Fichefet, T., Friedlingstein, P., et al. (2013). Long-term climate change: Projections, commitments and irreversibility. In *Climate change 2013: The physical science basis: Contribution of Working Group I to the Fifth Assessment Report of the Intergovernmental Panel on Climate Change* (pp. 1029–1136). Cambridge University Press.

Crutzen, P. J. (1970). The influence of nitrogen oxides on the atmospheric ozone content. *Quarterly Journal of the Royal Meteorological Society*, *96*(408), 320–325. https://doi.org/10.1002/qj.49709640815

Dacic, N., Sullivan, J. T., Knowland, K. E., Wolfe, G. M., Oman, L. D., Berkoff, T. A., & Gronoff, G. P. (2020). Evaluation of NASA's high-resolution global composition simulations: Understanding a pollution event in the Chesapeake Bay during the summer 2017 OWLETS campaign. *Atmospheric Environment*, *222*, 117133. https://doi.org/10.1016/j.atmosenv.2019.117133

Dameris, M., Loyola, D. G., Nützel, M., Coldewey-Egbers, M., Lerot, C., Romahn, F., & van Roozendael, M. (2021). Record low ozone values over the Arctic in boreal spring 2020. *Atmospheric Chemistry and Physics*, *21*(2), 617–633. https://doi.org/10.5194/acp-21-617-2021

Daniel, J., Velders, G., Douglass, A., Forster, P., Hauglustaine, D., Isaksen, I., et al. (2006). Halocarbon scenarios, ozone depletion potentials, and global warming potentials (chapter 8). In *Scientific assessment of ozone depletion: 2006. Global Ozone Research and Monitoring Project—Report No. 50* (pp. 8–1).

Darmenov, A., & da Silva, A. (2015). *The Quick Fire Emissions Dataset (QFED): Documentation of versions 2.1, 2.2 and 2.4* (Technical Report, Vol. 38). NASA/TM–2015–104606.

Davis, S. M., Hegglin, M. I., Fujiwara, M., Dragani, R., Harada, Y., Kobayashi, C., et al. (2017). Assessment of upper tropospheric and stratospheric water vapor and ozone in reanalyses as part of S-RIP. *Atmospheric Chemistry and Physics*, *17*(20), 12743–12778. https://doi.org/10.5194/acp-17-12743-2017

DeLand, M. T., Bhartia, P. K., Kramarova, N., & Chen, Z. (2020). OMPS LP observations of PSC variability during the NH 2019–2020 season. *Geophysical Research Letters*, *47*(20), e2020GL090216. https://doi.org/10.1029/2020GL090216

Douglass, A. R., Prather, M. J., Hall, T. M., Strahan, S. E., Rasch, P. J., Sparling, L. C., et al. (1999). Choosing meteorological input for the global modeling initiative assessment of high-speed aircraft. *Journal of Geophysical Research*, *104*(D22), 27545–27564. https://doi.org/10.1029/1999JD900827

Douglass, A. R., Stolarski, R. S., Strahan, S. E., & Connell, P. S. (2004). Radicals and reservoirs in the GMI chemistry and transport model: Comparison to measurements. *Journal of Geophysical Research*, *109*(D16), D16302. https://doi.org/10.1029/2004JD004632

Duncan, B. N., Malings, C. A., Knowland, K. E., Anderson, D. C., Prados, A. I., Keller, C. A., et al. (2021). Augmenting the standard operating procedures of health and air quality stakeholders with NASA resources. *GeoHealth*, *5*(9), e2021GH000451. https://doi.org/10.1029/2021GH000451

Duncan, B. N., Strahan, S. E., Yoshida, Y., Steenrod, S. D., & Livesey, N. (2007). Model study of the cross-tropopause transport of biomass burning pollution. *Atmospheric Chemistry and Physics*, *7*(14), 3713–3736. https://doi.org/10.5194/acp-7-3713-2007

Dupuy, E., Walker, K. A., Kar, J., Boone, C. D., McElroy, C. T., Bernath, P. F., et al. (2009). Validation of ozone measurements from the Atmospheric Chemistry Experiment (ACE). *Atmospheric Chemistry and Physics*, *9*(2), 287–343. https://doi.org/10.5194/acp-9-287-2009

Eastham, S. D., Weisenstein, D. K., & Barrett, S. R. (2014). Development and evaluation of the unified tropospheric–stratospheric chemistry extension (UCX) for the global chemistry-transport model GEOS-Chem. *Atmospheric Environment*, *89*, 52–63. https://doi.org/10.1016/j.atmosenv.2014.02.001

Engel, A., & Rigby, M. (2018). *Update on ozone-depleting substances (ODSs) and other gases of interest to the Montreal Protocol, Chapter 1 in Scientific Assessment of Ozone Depletion: 2018. Global Ozone Research and Monitoring Project — Report No. 58*. Retrieved from https://csl.noaa.gov/assessments/ozone/2018/downloads/Chapter1_2018OzoneAssessment.pdf

Errera, Q., Chabrillat, S., Christophe, Y., Debosscher, J., Hubert, D., Lahoz, W., et al. (2019). Technical note: Reanalysis of Aura MLS chemical observations. *Atmospheric Chemistry and Physics*, *19*(21), 13647–13679. https://doi.org/10.5194/acp-19-13647-2019

Eyring, V., Shepherd, T. G., & Waugh, D. W. (Eds.). (2010). *SPARC CCMVal report on the evaluation of chemistry-climate models* (Technical Report, Vol. 5). SPARC. Retrieved from http://www.sparc-climate.org/publications/sparc-reports/

Farman, J. C., Gardiner, B. G., & Shanklin, J. D. (1985). Large losses of total ozone in Antarctica reveal seasonal ClO_x/NO_x interaction. *Nature*, *315*(6016), 207–210. https://doi.org/10.1038/315207a0

Feng, W., Dhomse, S. S., Arosio, C., Weber, M., Burrows, J. P., Santee, M. L., & Chipperfield, M. P. (2021). Arctic ozone depletion in 2019/20: Roles of chemistry, dynamics and the Montreal Protocol. *Geophysical Research Letters*, *48*(4), e2020GL091911. https://doi.org/10.1029/2020GL091911

Frith, S. M., Kramarova, N. A., Stolarski, R. S., McPeters, R. D., Bhartia, P. K., & Labow, G. J. (2014). Recent changes in total column ozone based on the SBUV Version 8.6 Merged Ozone Data Set. *Journal of Geophysical Research*, *119*(16), 9735–9751. https://doi.org/10.1002/2014JD021889

Funke, B., López-Puertas, M., Gil-López, S., von Clarmann, T., Stiller, G. P., Fischer, H., & Kellmann, S. (2005). Downward transport of upper atmospheric NO_x into the polar stratosphere and lower mesosphere during the Antarctic 2003 and Arctic 2002/2003 winters. *Journal of Geophysical Research*, *110*(D24), D24308. https://doi.org/10.1029/2005JD006463

Gronoff, G., Berkoff, T., Knowland, K., Lei, L., Shook, M., Fabbri, B., et al. (2021). Case study of stratospheric intrusion above Hampton, Virginia: Lidar-observation and modeling analysis. *Atmospheric Environment*, 118498. https://doi.org/10.1016/j.atmosenv.2021.118498

Grooß, J.-U., Müller, R., Spang, R., Tritscher, I., Wegner, T., Chipperfield, M. P., et al. (2018). On the discrepancy of HCl processing in the core of the wintertime polar vortices. *Atmospheric Chemistry and Physics*, *18*(12), 8647–8666. https://doi.org/10.5194/acp-18-8647-2018

Hanson, D. R., & Ravishankara, A. R. (1992). Heterogeneous chemistry of hydrogen bromide and hydrogen fluoride. *The Journal of Physical Chemistry*, *96*(23), 9441–9446. https://doi.org/10.1021/j100202a069

Hanson, D. R., & Ravishankara, A. R. (1995). Heterogeneous chemistry of bromine species in sulfuric acid under stratospheric conditions. *Geophysical Research Letters*, *22*(4), 385–388. https://doi.org/10.1029/94GL03379

Holton, J. R. (1986). A dynamically based transport parameterization for one-dimensional photochemical models of the stratosphere. *Journal of Geophysical Research*, *91*(D2), 2681–2686. https://doi.org/10.1029/JD091iD02p02681

Hu, L., Keller, C. A., Long, M. S., Sherwen, T., Auer, B., Da Silva, A., et al. (2018). Global simulation of tropospheric chemistry at 12.5 km resolution: Performance and evaluation of the GEOS-Chem chemical module (v10-1) within the NASA GEOS Earth system model (GEOS-5 ESM). *Geoscientific Model Development*, *11*(11), 4603–4620. https://doi.org/10.5194/gmd-11-4603-2018

Inness, A., Chabrillat, S., Flemming, J., Huijnen, V., Langenrock, B., Nicolas, J., et al. (2020). Exceptionally low Arctic stratospheric ozone in spring 2020 as seen in the CAMS reanalysis. *Journal of Geophysical Research: Atmospheres*, *125*(23), e2020JD033563. https://doi.org/10.1029/2020JD033563

Jin, J. J., Semeniuk, K., Beagley, S. R., Fomichev, V. I., Jonsson, A. I., McConnell, J. C., et al. (2009). Comparison of CMAM simulations of carbon monoxide (CO), nitrous oxide (N_2O), and methane (CH_4) with observations from Odin/SMR, ACE-FTS, and Aura/MLS. *Atmospheric Chemistry and Physics*, *9*(10), 3233–3252. https://doi.org/10.5194/acp-9-3233-2009

Johnson, M. S., Strawbridge, K., Knowland, K. E., Keller, C., & Travis, M. (2021). Long-range transport of Siberian biomass burning emissions to North America during FIREX-AQ. *Atmospheric Environment*, *252*, 118241. https://doi.org/10.1016/j.atmosenv.2021.118241

Keene, W. C., Khalil, M. A. K., Erickson, D. J., III, McCulloch, A., Graedel, T. E., Lobert, J. M., et al. (1999). Composite global emissions of reactive chlorine from anthropogenic and natural sources: Reactive Chlorine Emissions Inventory. *Journal of Geophysical Research*, *104*(D7), 8429–8440. https://doi.org/10.1029/1998JD100084

Keller, C. A., Knowland, K. E., Duncan, B. N., Liu, J., Anderson, D. C., Das, S., et al. (2021). Description of the NASA GEOS Composition Forecast Modeling System GEOS-CF v1.0. *Journal of Advances in Modeling Earth Systems*, *13*(4), e2020MS002413. https://doi.org/10.1029/2020MS002413

Keller, C. A., Long, M. S., Yantosca, R. M., Da Silva, A. M., Pawson, S., & Jacob, D. J. (2014). HEMCO v1.0: A versatile, ESMF-compliant component for calculating emissions in atmospheric models. *Geoscientific Model Development*, *7*(4), 1409–1417. https://doi.org/10.5194/gmd-7-1409-2014

Kinnison, D. E., Connell, P. S., Rodriguez, J. M., Rotman, D. A., Considine, D. B., Tannahill, J., et al. (2001). The global modeling initiative assessment model: Application to high-speed civil transport perturbation. *Journal of Geophysical Research*, *106*(D2), 1693–1711. https://doi.org/10.1029/2000JD900406

Kirner, O., Ruhnke, R., Buchholz-Dietsch, J., Jöckel, P., Brühl, C., & Steil, B. (2011). Simulation of polar stratospheric clouds in the chemistry-climate-model EMAC via the submodel PSC. *Geoscientific Model Development*, *4*(1), 169–182. https://doi.org/10.5194/gmd-4-169-2011

Knowland, K. E., Keller, C. A., & Lucchesi, R. (2022). *File Specification for GEOS-CF Products, GMAO Office Note No. 17 (Version 1.2)* (p. 53). Retrieved from http://gmao.gsfc.nasa.gov/pubs/office_notes.php

Knowland, K. E., Ott, L. E., Duncan, B. N., & Wargan, K. (2017). Stratospheric intrusion-influenced ozone air quality exceedances investigated in the NASA MERRA-2 reanalysis. *Geophysical Research Letters*, *44*(20), 10691–10701. https://doi.org/10.1002/2017GL074532

Koike, M., Kondo, Y., Takegawa, N., Lefevre, F., Ikeda, H., Irie, H., et al. (2002). Redistribution of reactive nitrogen in the Arctic lower stratosphere in the 1999/2000 winter. *Journal of Geophysical Research*, *107*(D20). https://doi.org/10.1029/2001JD001089

Krzyzanowski, M., & Cohen, A. (2008). Update of WHO air quality guidelines. *Air Quality, Atmosphere & Health*, *1*, 7–13. https://doi.org/10.1007/s11869-008-0008-9

Kuang, S., Newchurch, M. J., Burris, J., Wang, L., Knupp, K., & Huang, G. (2012). Stratosphere-to-troposphere transport revealed by ground-based lidar and ozonesonde at a midlatitude site. *Journal of Geophysical Research*, *117*(D18). https://doi.org/10.1029/2012JD017695

Kuang, S., Newchurch, M. J., Johnson, M. S., Wang, L., Burris, J., Pierce, R. B., et al. (2017). Summertime tropospheric ozone enhancement associated with a cold front passage due to stratosphere-to-troposphere transport and biomass burning: Simultaneous ground-based lidar and airborne measurements. *Journal of Geophysical Research: Atmospheres*, *122*(2), 1293–1311. https://doi.org/10.1002/2016JD026078

Langford, A. O., Aikin, K. C., Eubank, C. S., & Williams, E. J. (2009). Stratospheric contribution to high surface ozone in Colorado during springtime. *Geophysical Research Letters*, *36*(12), L12801. https://doi.org/10.1029/2009GL038367

Lawrence, Z. D., Manney, G. L., & Wargan, K. (2018). Reanalysis intercomparisons of stratospheric polar processing diagnostics. *Atmospheric Chemistry and Physics*, *18*(18), 13547–13579. https://doi.org/10.5194/acp-18-13547-2018

Lawrence, Z. D., Perlwitz, J., Butler, A. H., Manney, G. L., Newman, P. A., Lee, S. H., & Nash, E. R. (2020). The remarkably strong Arctic stratospheric polar vortex of winter 2020: Links to record-breaking Arctic oscillation and ozone loss. *Journal of Geophysical Research: Atmospheres*, *125*(22), e2020JD033271. https://doi.org/10.1029/2020JD033271

Leblanc, T., Brewer, M. A., Wang, P. S., Granados-Muñoz, M. J., Strawbridge, K. B., Travis, M., et al. (2018). Validation of the TOLNet lidars: The Southern California Ozone Observation Project (SCOOP). *Atmospheric Measurement Techniques*, *11*(11), 6137–6162. https://doi.org/10.5194/amt-11-6137-2018

Lecouffe, A., Godin-Beekmann, S., Pazmiño, A., & Hauchecorne, A. (2022). Evolution of the intensity and duration of the Southern Hemisphere stratospheric polar vortex edge for the period 1979–2020. *Atmospheric Chemistry and Physics*, *22*(6), 4187–4200. https://doi.org/10.5194/acp-22-4187-2022

Le Quéré, C., Jackson, R. B., Jones, M. W., Smith, A. J. P., Abernethy, S., Andrew, R. M., et al. (2020). Temporary reduction in daily global CO_2 emissions during the COVID-19 forced confinement. *Nature Climate Change*, *10*(7), 647–653. https://doi.org/10.1038/s41558-020-0797-x

Levelt, P. F., Joiner, J., Tamminen, J., Veefkind, J. P., Bhartia, P. K., Stein Zweers, D. C., et al. (2018). The ozone monitoring instrument: Overview of 14 years in space. *Atmospheric Chemistry and Physics*, *18*(8), 5699–5745. https://doi.org/10.5194/acp-18-5699-2018

Levelt, P. F., van den Oord, G. H. J., Dobber, M. R., Malkki, A., Visser, H., de Vries, J., et al. (2006). The ozone monitoring instrument. *IEEE Transactions on Geoscience and Remote Sensing*, *44*(5), 1093–1101. https://doi.org/10.1109/TGRS.2006.872333

Livesey, N. J., Read, W. G., Froidevaux, L., Lambert, A., Santee, M. L., Schwartz, M. J., et al. (2021). Investigation and amelioration of long-term instrumental drifts in water vapor and nitrous oxide measurements from the Aura Microwave Limb Sounder (MLS) and their implications for studies of variability and trends. *Atmospheric Chemistry and Physics*, *21*(20), 15409–15430. https://doi.org/10.5194/acp-21-15409-2021

Livesey, N. J., Read, W. G., Wagner, P. A., Froidevaux, L., Santee, M. L., Schwartz, M. J., et al. (2020). *Version 5.0x Level 2 and 3 data quality and description document, JPL D-105336 Rev. A*. Retrieved from https://mls.jpl.nasa.gov/data/v5-0_data_quality_document.pdf

Long, M. S., Yantosca, R., Nielsen, J. E., Keller, C. A., da Silva, A., Sulprizio, M. P., et al. (2015). Development of a grid-independent GEOS-Chem chemical transport model (v9-02) as an atmospheric chemistry module for Earth system models. *Geoscientific Model Development*, *8*(3), 595–602. https://doi.org/10.5194/gmd-8-595-2015

Lucchesi, R. (2015). *File specification for GEOS-5 FP-IT, GMAO Office Note No. 2 (Version 1.4)*. Retrieved from http://gmao.gsfc.nasa.gov/pubs/office_notes.php

Lucchesi, R. (2018). *File specification for GEOS FP, GMAO Office Note No. 4 (Version 1.2)* (p. 61). Retrieved from http://gmao.gsfc.nasa.gov/pubs/office_notes.php

Mahlman, J. D., Levy, H., II, & Moxim, W. J. (1986). Three-dimensional simulations of stratospheric N_2O: Predictions for other trace constituents. *Journal of Geophysical Research*, *91*(D2), 2687–2707. https://doi.org/10.1029/JD091iD02p02687

Manney, G. L., Harwood, R. S., MacKenzie, I. A., Minschwaner, K., Allen, D. R., Santee, M. L., et al. (2009). Satellite observations and modeling of transport in the upper troposphere through the lower mesosphere during the 2006 major stratospheric sudden warming. *Atmospheric Chemistry and Physics*, *9*(14), 4775–4795. https://doi.org/10.5194/acp-9-4775-2009

Manney, G. L., Livesey, N. J., Santee, M. L., Froidevaux, L., Lambert, A., Lawrence, Z. D., et al. (2020). Record-low Arctic stratospheric ozone in 2020: MLS observations of chemical processes and comparisons with previous extreme winters. *Geophysical Research Letters*, *47*(16), e2020GL089063. https://doi.org/10.1029/2020GL089063

Manney, G. L., Zurek, R. W., O'Neill, A., & Swinbank, R. (1994). On the motion of air through the stratospheric polar vortex. *Journal of the Atmospheric Sciences*, *51*(20), 2973–2994. https://doi.org/10.1175/1520-0469(1994)051<2973:OTMOAT>2.0.CO;2

Mauldin, L. E., Salikhov, R., Habib, S., Vladimirov, A. G., Carraway, D., Petrenko, G., & Comella, J. (1998). Meteor-3M(1)/Stratospheric Aerosol and Gas Experiment III (SAGE III) jointly sponsored by the National Aeronautics and Space Administration and the Russian Space Agency. *Proceedings of SPIE*, *3501*, 355–365. https://doi.org/10.1117/12.317767

McCormick, M. P., & Chu, W. P. (2004). *Stratospheric aerosol and gas experiment III (SAGE III): Data product user's guide. Version 1.5*. National Aeronautics and Space Administration.

McCormick, M. P., Lei, L., Hill, M. T., Anderson, J., Querel, R., & Steinbrecht, W. (2020). Early results and validation of SAGE III-ISS ozone profile measurements from onboard the International Space Station. *Atmospheric Measurement Techniques*, *13*(3), 1287–1297. https://doi.org/10.5194/amt-13-1287-2020

McDermid, I. S., Beyerle, G., Haner, D. A., & Leblanc, T. (2002). Redesign and improved performance of the tropospheric ozone lidar at the Jet Propulsion Laboratory Table Mountain Facility. *Applied Optics*, *41*(36), 7550–7555. https://doi.org/10.1364/AO.41.007550

McPeters, R., Kroon, M., Labow, G., Brinksma, E., Balis, D., Petropavlovskikh, I., et al. (2008). Validation of the Aura Ozone Monitoring Instrument total column ozone product. *Journal of Geophysical Research*, *113*(D15), D15S14. https://doi.org/10.1029/2007JD008802

Molina, M. J., & Rowland, F. S. (1974a). Predicted present stratospheric abundances of chlorine species from photodissociation of carbon tetrachloride. *Geophysical Research Letters*, *1*(7), 309–312. https://doi.org/10.1029/GL001i007p00309

Molina, M. J., & Rowland, F. S. (1974b). Stratospheric sink for chlorofluoromethanes: Chlorine atom-catalysed destruction of ozone. *Nature*, *249*(5460), 810–812. https://doi.org/10.1038/249810a0

Molod, A., Takacs, L., Suarez, M., & Bacmeister, J. (2015). Development of the GEOS-5 atmospheric general circulation model: Evolution from MERRA to MERRA2. *Geoscientific Model Development*, *8*(5), 1339–1356. https://doi.org/10.5194/gmd-8-1339-2015

Murray, L. T., Jacob, D. J., Logan, J. A., Hudman, R. C., & Koshak, W. J. (2012). Optimized regional and interannual variability of lightning in a global chemical transport model constrained by LIS/OTD satellite data. *Journal of Geophysical Research*, *117*(D20). https://doi.org/10.1029/2012JD017934

Nielsen, J. E., Pawson, S., Molod, A., Auer, B., da Silva, A. M., Douglass, A. R., et al. (2017). Chemical mechanisms and their applications in the Goddard Earth Observing System (GEOS) Earth System Model. *Journal of Advances in Modeling Earth Systems*, *9*(8), 3019–3044. https://doi.org/10.1002/2017MS001011

Orbe, C., Oman, L. D., Strahan, S. E., Waugh, D. W., Pawson, S., Takacs, L. L., & Molod, A. M. (2017). Large-scale atmospheric transport in GEOS replay simulations. *Journal of Advances in Modeling Earth Systems*, *9*(7), 2545–2560. https://doi.org/10.1002/2017MS001053

Ott, L. E., Duncan, B. N., Thompson, A. M., Diskin, G., Fasnacht, Z., Langford, A. O., et al. (2016). Frequency and impact of summertime stratospheric intrusions over Maryland during DISCOVER-AQ (2011): New evidence from NASA's GEOS-5 simulations. *Journal of Geophysical Research: Atmospheres*, *121*(7), 3687–3706. https://doi.org/10.1002/2015JD024052

Parrella, J. P., Jacob, D. J., Liang, Q., Zhang, Y., Mickley, L. J., Miller, B., et al. (2012). Tropospheric bromine chemistry: Implications for present and pre-industrial ozone and mercury. *Atmospheric Chemistry and Physics*, *12*(15), 6723–6740. https://doi.org/10.5194/acp-12-6723-2012

Plumb, R. A. (2007). Tracer interrelationships in the stratosphere. *Reviews of Geophysics*, *45*(4). https://doi.org/10.1029/2005RG000179

Prather, M. J., Ehhalt, D., Dentener, F., Derwent, R., Dlugokencky, E., Holland, E., et al. (2001). Atmospheric chemistry and greenhouse gases. In J. T. Houghton, Y. Ding, D. J. Griggs, M. Noguer, P. J. van der Linden, X. Dai, et al. (Eds.), *Climate change 2001: The scientific basis. Contribution of Working Group 1 to the Third Assessment Report of the Intergovernmental Panel on Climate Change* (pp. 239–288). Cambridge University Press.

Randall, C. E., Harvey, V. L., Manney, G. L., Orsolini, Y., Codrescu, M., Sioris, C., et al. (2005). Stratospheric effects of energetic particle precipitation in 2003–2004. *Geophysical Research Letters*, *32*(5), L05802. https://doi.org/10.1029/2004GL022003

Randall, C. E., Harvey, V. L., Singleton, C. S., Bailey, S. M., Bernath, P. F., Codrescu, M., et al. (2007). Energetic particle precipitation effects on the Southern Hemisphere stratosphere in 1992–2005. *Journal of Geophysical Research*, *112*(D8), D08308. https://doi.org/10.1029/2006JD007696

Reimann, S., Elkins, J. W., Fraser, P. J., Hall, B. D., Kurylo, M. J., Mahieu, E., et al. (2018). Observing the atmospheric evolution of ozone-depleting substances. *Comptes Rendus Geoscience*, *350*(7), 384–392. (30th Anniversary of the Montreal Protocol: From the safeguard of the ozone layer to the protection of the Earth Climate). https://doi.org/10.1016/j.crte.2018.08.008

Robinson, J., Kotsakis, A., Santos, F., Swap, R., Knowland, K., Labow, G., et al. (2020). Using networked Pandora observations to capture spatiotemporal changes in total column ozone associated with stratosphere-to-troposphere transport. *Atmospheric Research*, *238*, 104872. https://doi.org/10.1016/j.atmosres.2020.104872

Rotman, D. A., Tannahill, J. R., Kinnison, D. E., Connell, P. S., Bergmann, D., Proctor, D., et al. (2001). Global Modeling Initiative assessment model: Model description, integration, and testing of the transport shell. *Journal of Geophysical Research*, *106*(D2), 1669–1691. https://doi.org/10.1029/2000JD900463

Rowland, F. S., Spencer, J. E., & Molina, M. J. (1976). Stratospheric formation and photolysis of chlorine nitrate. *The Journal of Physical Chemistry*, *80*(24), 2711–2713. https://doi.org/10.1021/j100565a019

Ruiz, D. J., Prather, M. J., Strahan, S. E., Thompson, R. L., Froidevaux, L., & Steenrod, S. D. (2021). How atmospheric chemistry and transport drive surface variability of N_2O and CFC-11. *Journal of Geophysical Research: Atmospheres*, *126*(8), e2020JD033979. https://doi.org/10.1029/2020JD033979

Salawitch, R. J., Gobbi, G. P., Wofsy, S. C., & McElroy, M. B. (1989). Denitrification in the Antarctic stratosphere. *Nature*, *339*(6225), 525–527. https://doi.org/10.1038/339525a0

Sander, S. P., Friedl, R. R., Barker, J. R., Burkholder, J. B., Friedl, R. R., Golden, D. M., et al. (2011). *Chemical kinetics and photochemical data for use in atmospheric studies, evaluation number 17, JPL Publication 10-6*. Jet Propulsion Laboratory. Retrieved from http://jpldataeval.jpl.nasa.gov

Schlink, U., Herbarth, O., Richter, M., Dorling, S., Nunnari, G., Cawley, G., & Pelikan, E. (2006). Statistical models to assess the health effects and to forecast ground-level ozone. *Environmental Modelling & Software*, *21*(4), 547–558. https://doi.org/10.1016/j.envsoft.2004.12.002

Schmidt, J. A., Jacob, D. J., Horowitz, H. M., Hu, L., Sherwen, T., Evans, M. J., et al. (2016). Modeling the observed tropospheric BrO background: Importance of multiphase chemistry and implications for ozone, OH, and mercury. *Journal of Geophysical Research: Atmospheres*, *121*(19), 11819–11835. https://doi.org/10.1002/2015JD024229

Sheese, P. E., Walker, K. A., Boone, C. D., Bernath, P. F., Froidevaux, L., Funke, B., et al. (2017). ACE-FTS ozone, water vapour, nitrous oxide, nitric acid, and carbon monoxide profile comparisons with MIPAS and MLS. *Journal of Quantitative Spectroscopy and Radiative Transfer*, *186*, 63–80. https://doi.org/10.1016/j.jqsrt.2016.06.026

Sheese, P. E., Walker, K. A., Boone, C. D., Bourassa, A. E., Degenstein, D. A., Froidevaux, L., et al. (2022). Assessment of the quality of ACE-FTS stratospheric ozone data. *Atmospheric Measurement Techniques*, *15*(5), 1233–1249. https://doi.org/10.5194/amt-15-1233-2022

Sherwen, T., Evans, M. J., Carpenter, L. J., Andrews, S. J., Lidster, R. T., Dix, B., et al. (2016). Iodine's impact on tropospheric oxidants: A global model study in GEOS-Chem. *Atmospheric Chemistry and Physics*, *16*(2), 1161–1186. https://doi.org/10.5194/acp-16-1161-2016

Sherwen, T., Schmidt, J. A., Evans, M. J., Carpenter, L. J., Großmann, K., Eastham, S. D., et al. (2016). Global impacts of tropospheric halogens (Cl, Br, I) on oxidants and composition in GEOS-Chem. *Atmospheric Chemistry and Physics*, *16*(18), 12239–12271. https://doi.org/10.5194/acp-16-12239-2016

Siskind, D. E., Bacmeister, J. T., Summers, M. E., & Russell, J. M. III, (1997). Two-dimensional model calculations of nitric oxide transport in the middle atmosphere and comparison with Halogen Occultation Experiment data. *Journal of Geophysical Research*, *102*(D3), 3527–3545. https://doi.org/10.1029/96JD02970

Siskind, D. E., Stevens, M. H., Englert, C. R., & Mlynczak, M. G. (2013). Comparison of a photochemical model with observations of mesospheric hydroxyl and ozone. *Journal of Geophysical Research: Atmospheres*, *118*(1), 195–207. https://doi.org/10.1029/2012JD017971

Skachko, S., Ménard, R., Errera, Q., Christophe, Y., & Chabrillat, S. (2016). EnKF and 4D-Var data assimilation with chemical transport model BASCOE (version 05.06). *Geoscientific Model Development*, *9*(8), 2893–2908. https://doi.org/10.5194/gmd-9-2893-2016

Solomon, S., Crutzen, P. J., & Roble, R. G. (1982). Photochemical coupling between the thermosphere and the lower atmosphere: 1. Odd nitrogen from 50 to 120 km. *Journal of Geophysical Research*, *87*(C9), 7206–7220. https://doi.org/10.1029/JC087iC09p07206

Solomon, S., Garcia, R. R., Rowland, F. S., & Wuebbles, D. J. (1986). On the depletion of Antarctic ozone. *Nature*, *321*(6072), 755–758. https://doi.org/10.1038/321755a0

Stauffer, R. M., Thompson, A. M., Kollonige, D. E., Witte, J. C., Tarasick, D. W., Davies, J., et al. (2020). A post-2013 dropoff in total ozone at a third of global ozonesonde stations: Electrochemical concentration cell instrument artifacts? *Geophysical Research Letters*, *47*(11), e2019GL086791. https://doi.org/10.1029/2019GL086791

Stauffer, R. M., Thompson, A. M., Oman, L. D., & Strahan, S. E. (2019). The effects of a 1998 observing system change on MERRA-2-based ozone profile simulations. *Journal of Geophysical Research*, *124*(13), 7429–7441. https://doi.org/10.1029/2019JD030257

Steinbrecht, W., Kubistin, D., Plass-Dülmer, C., Davies, J., Tarasick, D. W., von der Gathen, P., et al. (2021). COVID-19 crisis reduces free tropospheric ozone across the Northern Hemisphere. *Geophysical Research Letters*, *48*(5), e2020GL091987. https://doi.org/10.1029/2020GL091987

Sterling, C. W., Johnson, B. J., Oltmans, S. J., Smit, H. G. J., Jordan, A. F., Cullis, P. D., et al. (2018). Homogenizing and estimating the uncertainty in NOAA's long-term vertical ozone profile records measured with the electrochemical concentration cell ozonesonde. *Atmospheric Measurement Techniques*, *11*(6), 3661–3687. https://doi.org/10.5194/amt-11-3661-2018

Stolarski, R. S., & Cicerone, R. J. (1974). Stratospheric chlorine: A possible sink for ozone. *Canadian Journal of Chemistry*, *52*(8), 1610–1615. https://doi.org/10.1139/v74-233

Stolarski, R. S., Krueger, A. J., Schoeberl, M. R., McPeters, R. D., Newman, P. A., & Alpert, J. C. (1986). Nimbus 7 satellite measurements of the springtime Antarctic ozone decrease. *Nature*, *322*(6082), 808–811. https://doi.org/10.1038/322808a0

Strahan, S. E., & Douglass, A. R. (2018). Decline in Antarctic ozone depletion and lower stratospheric chlorine determined from Aura Microwave Limb Sounder observations. *Geophysical Research Letters*, *45*(1), 382–390. https://doi.org/10.1002/2017GL074830

Strahan, S. E., Duncan, B. N., & Hoor, P. (2007). Observationally derived transport diagnostics for the lowermost stratosphere and their application to the GMI chemistry and transport model. *Atmospheric Chemistry and Physics*, *7*(9), 2435–2445. https://doi.org/10.5194/acp-7-2435-2007

Strode, S. A., Rodriguez, J. M., Logan, J. A., Cooper, O. R., Witte, J. C., Lamsal, L. N., et al. (2015). Trends and variability in surface ozone over the United States. *Journal of Geophysical Research: Atmospheres*, *120*(17), 9020–9042. https://doi.org/10.1002/2014JD022784

Thompson, A. M., Witte, J. C., Sterling, C., Jordan, A., Johnson, B. J., Oltmans, S. J., et al. (2017). First reprocessing of Southern Hemisphere Additional Ozonesondes (SHADOZ) ozone profiles (1998–2016): 2. Comparisons with satellites and ground-based instruments. *Journal of Geophysical Research: Atmospheres*, *122*(23), 13000–13025. https://doi.org/10.1002/2017JD027406

Toon, O. B., Turco, R. P., & Hamill, P. (1990). Denitrification mechanisms in the polar stratospheres. *Geophysical Research Letters*, *17*(4), 445–448. https://doi.org/10.1029/GL017i004p00445

Turner, E. C., Manners, J., Morcrette, C. J., O'Hagan, J. B., & Smedley, A. R. D. (2017). Toward a New UV Index Diagnostic in the Met Office's Forecast Model. *Journal of Advances in Modeling Earth Systems*, *9*(7), 2654–2671. https://doi.org/10.1002/2017MS001050

Wang, H. J. R., Damadeo, R., Flittner, D., Kramarova, N., Taha, G., Davis, S., et al. (2020). Validation of SAGE III/ISS Solar Occultation Ozone Products With Correlative Satellite and Ground-Based Measurements. *Journal of Geophysical Research: Atmospheres*, *125*(11), e2020JD032430. https://doi.org/10.1029/2020JD032430

Wang, L., Newchurch, M. J., Alvarez, R. J., II, Berkoff, T. A., Brown, S. S., Carrion, W., et al. (2017). Quantifying TOLNet ozone lidar accuracy during the 2014 DISCOVER-AQ and FRAPPÉ campaigns. *Atmospheric Measurement Techniques*, *10*(10), 3865–3876. https://doi.org/10.5194/amt-10-3865-2017

Wargan, K., Kramarova, N., Weir, B., Pawson, S., & Davis, S. M. (2020). Toward a reanalysis of stratospheric ozone for trend studies: Assimilation of the Aura Microwave Limb Sounder and Ozone Mapping and Profiler Suite Limb Profiler data. *Journal of Geophysical Research: Atmospheres*, *125*(4), e2019JD031892. https://doi.org/10.1029/2019JD031892

Wargan, K., Labow, G., Frith, S., Pawson, S., Livesey, N., & Partyka, G. (2017). Evaluation of the ozone fields in NASA's MERRA-2 reanalysis. *Journal of Climate*, *30*(8), 2961–2988. https://doi.org/10.1175/JCLI-D-16-0699.1

Wargan, K., Orbe, C., Pawson, S., Ziemke, J. R., Oman, L. D., Olsen, M. A., et al. (2018). Recent decline in extratropical lower stratospheric ozone attributed to circulation changes. *Geophysical Research Letters*, *45*(10), 5166–5176. https://doi.org/10.1029/2018GL077406

Wargan, K., Pawson, S., Olsen, M. A., Witte, J. C., Douglass, A. R., Ziemke, J. R., et al. (2015). The global structure of upper troposphere-lower stratosphere ozone in GEOS-5: A multiyear assimilation of EOS Aura data. *Journal of Geophysical Research: Atmospheres*, *120*(5), 2013–2036. https://doi.org/10.1002/2014JD022493

Wargan, K., Weir, B., Manney, G. L., Cohn, S. E., & Livesey, N. J. (2020). The anomalous 2019 Antarctic ozone hole in the GEOS Constituent Data Assimilation System with MLS observations. *Journal of Geophysical Research: Atmospheres*, *125*(18), e2020JD033335. https://doi.org/10.1029/2020JD033335

Waters, J. W., Froidevaux, L., Harwood, R. S., Jarnot, R. F., Pickett, H. M., Read, W. G., et al. (2006). The Earth observing system microwave limb sounder (EOS MLS) on the Aura satellite. *IEEE Transactions on Geoscience and Remote Sensing*, *44*(5), 1075–1092. https://doi.org/10.1109/tgrs.2006.873771

Waugh, D. (2009). The age of stratospheric air. *Nature Geoscience*, *2*(1), 14–16. https://doi.org/10.1038/ngeo397

Weisenstein, D. K., Yue, G. K., Ko, M. K., Sze, N.-D., Rodriguez, J. M., & Scott, C. J. (1997). A two-dimensional model of sulfur species and aerosols. *Journal of Geophysical Research*, *102*(D11), 13019–13035. https://doi.org/10.1029/97jd00901

Wetzel, G., Oelhaf, H., Ruhnke, R., Friedl-Vallon, F., Kleinert, A., Kouker, W., et al. (2002). NO_y partitioning and budget and its correlation with N_2O in the Arctic vortex and in summer midlatitudes in 1997. *Journal of Geophysical Research*, *107*(D16). ACH 3-1–ACH 3-10. https://doi.org/10.1029/2001JD000916

Wohltmann, I., von der Gathen, P., Lehmann, R., Maturilli, M., Deckelmann, H., Manney, G. L., et al. (2020). Near-complete local reduction of arctic stratospheric ozone by severe chemical loss in spring 2020. *Geophysical Research Letters*, *47*(20), e2020GL089547. https://doi.org/10.1029/2020GL089547

Zoogman, P., Liu, X., Suleiman, R. M., Pennington, W. F., Flittner, D. E., Al-Saadi, J. A., et al. (2017). Tropospheric emissions: Monitoring of pollution (TEMPO). *Journal of Quantitative Spectroscopy and Radiative Transfer*, *186*, 17–39. (Satellite Remote Sensing and Spectroscopy: Joint ACE-Odin Meeting, October 2015). https://doi.org/10.1016/j.jqsrt.2016.05.008